

# STAY Diffusion: Styled Layout Diffusion Model for Diverse Layout-to-Image Generation

Ruyu Wang<sup>1,2</sup> Xuefeng Hou<sup>1</sup> Sabrina Schmedding<sup>1</sup> Marco F. Huber<sup>2,3</sup>

<sup>1</sup>Bosch Center for Artificial Intelligence, Renningen, Germany

<sup>2</sup>Institute of Industrial Manufacturing and Management IFF, University of Stuttgart, Stuttgart, Germany

<sup>3</sup>Fraunhofer Institute for Manufacturing Engineering and Automation IPA, Stuttgart, Germany

{ruyu.wang, sabrina.schmedding}@de.bosch.com houxuefeng1997@gmail.com marco.huber@ieee.org

## Abstract

*In layout-to-image (L2I) synthesis, controlled complex scenes are generated from coarse information like bounding boxes. Such a task is exciting to many downstream applications because the input layouts offer strong guidance to the generation process while remaining easily reconfigurable by humans. In this paper, we proposed **ST**yled **LAY**out **Dif**fusion (**STAY** Diffusion), a diffusion-based model that produces photo-realistic images and provides fine-grained control of stylized objects in scenes. Our approach learns a global condition for each layout, and a self-supervised semantic map for weight modulation using a novel Edge-Aware Normalization (EA Norm). A new Styled-Mask Attention (SM Attention) is also introduced to cross-condition the global condition and image feature for capturing the objects' relationships. These measures provide consistent guidance through the model, enabling more accurate and controllable image generation. Extensive benchmarking demonstrates that our STAY Diffusion presents high-quality images while surpassing previous state-of-the-art methods in generation diversity, accuracy, and controllability.*

## 1. Introduction

Recently, deep generative models (DGMs) have advanced unprecedentedly on image synthesis tasks [7, 13, 28, 39, 40]. As multiple unconditional generative models [13, 17, 42] have shown a promising ability to capture data distribution and generate photo-realistic images, conditional generative models aim to achieve the same goal while conditioning the generated images with additional information. The given conditional information can range from coarse to detailed, such as class labels, text descriptions, semantic maps, or even other images, providing various levels of control during the generating process. Such control is favored in many practical applications like graphics editors or data augmentation with specific rare cases in medical or in-

dustrial domains. However, a trade-off exists between the flexibility for users and the strength of the model control signal: a text description may give little clues for object locations, whereas a semantic map can be hard to acquire and alter. In this respect, using layouts (i.e., a collection of labeled object bounding boxes) as the condition is an appealing solution since a layout offers guidance on object size and locations and is easier to access and reconfigure.

Despite the alluring traits, layout-to-image (L2I) synthesis poses a challenging task. It targets a one-to-many mapping problem involving generating multiple objects, capturing object interactions, and composing perceptually plausible scenes with the given layout. Early works [1, 41, 54] were primarily based on generative adversarial networks (GANs) due to their outstanding generation ability at the time. However, these models are prone to mode collapse and often fail to generate reasonable images with clear objects as illustrated in Fig. 1(a) (cf. bus in LostGAN v2 [41]). Some researchers addressed these problems by changing the network from CNN-based to transformer-based to better capture object relationships of a complex scene [50]. More recently, the advance of diffusion models (DMs) opened up new possibilities for high-resolution L2I synthesis. A few pioneer works have shown new impressive results by tokenizing the given layouts for their new attention mechanisms [34, 56] or by leveraging pretrained large text-to-image generation models (LTGMs) [6, 20].

In this work, we propose **ST**yled **LAY**out **Dif**fusion (STAY Diffusion), a diffusion-based L2I model providing fine-grained object control for diverse image synthesis as demonstrated in Fig. 1(b). Unlike prior works that tokenize [50, 56] or apply direct input concatenation to the layout [55], we learn a latent representation for each input object to predict pixel-wise object masks based on given layouts. The object representations consist of a category-specific part and an object-specific part that reflects its attribute (i.e., style). Such representations and their corre-

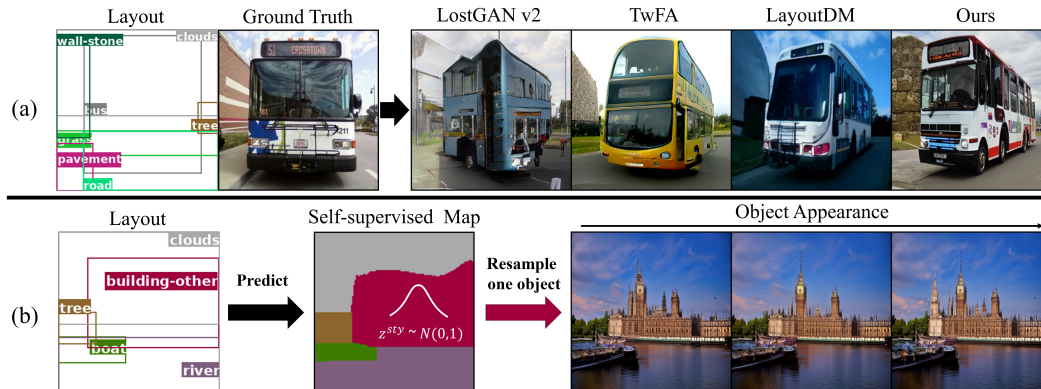


Figure 1. STAY Diffusion can produce high-quality images based on given bounding box layouts. (a) A comparison between STAY Diffusion and previous state-of-the-art methods. (b) In addition, STAY Diffusion learns a self-supervised semantic map for each layout and can manipulate object appearance by resampling its associated latent code  $z^{sty}$  (cf. the towers of the building).

sponding masks are used as the conditions for both the model’s normalization and attention layers. We thus refer to them as global conditions. Then, we introduce a new normalization method, termed Edge-Aware Normalization (EA Norm) to better utilize these global conditions. It embeds the object representations and their masks into the decoder of the diffusion network, where the overlapping areas of object masks are carefully processed for weight modulation. In addition to the EA Norm, a novel Styled-Mask Attention (SM Attention) mechanism is proposed to cross-condition object representations and image features, thereby enhancing object awareness and capturing object relationships in our model.

Extensive experiments on two benchmarking datasets, COCO-stuff [5] and Visual Genome (VG) [18], show that STAY Diffusion surpasses previous state-of-the-art (SOTA) methods in generation diversity, accuracy, and controllability, demonstrating the effectiveness of our proposed EA Norm and SM Attention.

Our contributions are summarized as follows:

- We propose a novel framework called **STyled LAYOut** Diffusion, a diffusion-based generative model for synthesizing high-fidelity and diverse images with precise control over multiple objects in complex scenes.
- Unlike other methods, we process the layouts into the global conditions (i.e., object representations and their predicted masks) and introduce two new modules—Edge-Aware Normalization and Styled-Mask Attention—utilizing the global conditions for fine-grained object control and scene understanding.
- The proposed STAY Diffusion produces high-quality images together with their self-supervised maps, while outperforming the previous SOTA methods regarding diversity, accuracy, and controllability in generation.

## 2. Related Works

**Conditional Image Synthesis.** Since the breakthrough in high-resolution photo-realistic image synthesis made by GANs [9], DGMs have attracted growing attention. While unconditional synthesis models [13, 17, 28, 39, 51] only take random noise as input and mainly focus on improving generation quality and capturing the underlying data distribution, conditional synthesis models [4, 7, 14, 23, 27, 31, 34] consider additional input signals (e.g., category, text, image) to achieve higher controllability along the generation process. Various ways to embed conditional signals into DGMs have been studied. For example, some works [29, 33] proposed to concatenate the conditions naively with input or intermediate network features, while others [11, 21, 41, 44] suggested injecting them in a projection-based way [25]. A popular trend is to modulate the normalization layers in models with conditional gains and bias [15, 30, 38], which are commonly used in semantic image synthesis. Our method is closely related to this approach, but instead of a semantic map, a layout as input is sufficient. Most early works conducted their investigations in GANs due to its superior performance at the time. Recently, DMs have emerged as the new SOTA family in image synthesis, where the ablated diffusion model (ADM) [7] first showed the promising prospect of DMs by outperforming GAN-based methods. Since then, many researchers have explored different ways such as guiding the generation process by conditional gradients [14] to condition DMs on additional information [2, 19, 22, 34, 45, 46]. Beside training a conditional DMs from scratch, leveraging pretrained LTGMs [24, 34, 36] for conditional image generation [26, 49, 52] is also a popular trend due to the resource efficiency and the rich expressiveness offered by large models.

**Layout-to-Image Synthesis.** L2I synthesis is one of the challenging tasks in conditional image synthesis, where

only coarse information (e.g., category, size, and location) of objects is given to compose a complex scene. Layouts, consisting of multiple labeled bounding boxes, were often used to aid other tasks like text-to-image synthesis prior to Layout2Im [54]. Attracted by the offered flexibility and controllability, researchers have explored many ways to adapt layouts into DGMs: LostGAN v2 [41] encode layouts into style features and object masks for ISLA Norm modulation. The following works [11, 21, 44] employed a similar mechanism to embed the layout information. Moreover, they introduced additional designs to tackle the object interaction and mask clarity for better generation quality. Apart from GAN-based models, Taming [16] and TwFA [50] used a pretrained VQ-GAN [8] as layout encoder and trained auto-regressive transformers on top to perform image generation. As a multimodal model, LDM [34] was the first DM to support L2I synthesis, demonstrating great potential to utilize DM as the backbone for such a task. More recently, three more dedicated DMs, LayoutDiffusion (LayoutDM) [56], LayoutDiffuse [6] and GLIGEN [20], were proposed. The first one introduced a novel module to better fuse the tokenized inputs (i.e., image and layout) for conditioning the model, while the other two leveraged a pretrained LTGM [34] for L2I generation to reduce training workload and exploit the rich semantic learned from large datasets. Our STAY Diffusion does not deploy pretrained LTGMs as in LayoutDiffuse or GLIGEN, allowing for higher adaptability when applying to domains beyond natural (e.g., medical or industrial) images. Instead of tokenizing layouts with additional models like in LayoutDM, we learn object representations and masks from layouts. The information is then treated as global conditions for both normalization and attention layers in our work.

### 3. Methodology

In this section, we present a novel framework named STAY Diffusion to transform coarse layout information into realistic images. Specifically, we refer to coarse layout information as a collection of bounding boxes and their categorical labels, which provides a rough sketch of a complex scene. Through the iterative diffusion steps, the proposed STAY Diffusion generates high-quality images from layouts. In the following, we begin with the model overview. Then, two crucial designs, Edge-Aware Normalization and Styled-Mask Attention, are introduced. Finally, we present the training and sampling methods for our framework.

#### 3.1. Layout-Conditional Diffusion Model

The overview of our model is illustrated in Fig. 2. A layout  $l$  is defined as a set of  $N$  objects, where each object is represented as  $o_i = \{b_i, c_i\}$ ,  $i = 1, \dots, N$ . Precisely,  $b_i = (x_0^i, y_0^i, h, w) \in [0, 1]^4$  denotes a bounding box in a normalized coordinate system and  $c_i \in \{1, \dots, C\}$  is the

object category. To account for the case where the number of objects in each layout is different, we introduce a padding class  $c = 0$  and set the coordinates as  $b_0 = (0, 0, 0, 0)$  to pad the number of objects in each layout to a predefined number. Consider a data point  $x_0$  sampled from a real data distribution  $q(\cdot)$  and a layout  $l$  as a condition: the goal of a conditional DM is to maximize the likelihood  $p_\theta(x_0|l)$  following the conditional data distribution  $q(x_0|l)$ . Two processes—the forward process and the reverse process—are defined to achieve the desired data generation. Starting from  $x_0$ , the forward process  $q(x_{1:T}|x_0)$  gradually adds a small amount of Gaussian noise at each timestep  $t$  according to

$$q(x_t|x_{t-1}) = \mathcal{N}(x_t; \sqrt{\alpha_t} \cdot x_{t-1}, (1 - \alpha_t) \cdot \mathbf{I}), \quad (1)$$

where  $1 - \alpha_t$  represents the noise magnitude. Assuming the added noise is from a diagonal Gaussian distribution and a sufficient amount is applied through the forward process, the acquired  $x_T$  can be approximated by  $\mathcal{N}(0, \mathbf{I})$ . On the other hand, the reverse process  $p_\theta(x_{0:T}|l)$  uses a parameterized network to estimate the real posterior  $q(x_{t-1}|x_t)$  by

$$p_\theta(x_{t-1}|x_t, l) = \mathcal{N}(x_{t-1}; \mu_\theta(x_t, l, t), \Sigma_\theta(x_t, l, t)), \quad (2)$$

progressively predicting a less noisy image at each step to recover  $x_0$ . Following Ho et al. [13], the optimization objective of the conditional DM can be simplified as

$$\mathcal{L}(\theta) = \mathbb{E}_{t, x_0, l, \epsilon} [\|\epsilon - \epsilon_\theta(x_t, l, t)\|^2], \quad (3)$$

where  $\epsilon$  is the added noise in the forward process at each timestep  $t$  and  $\epsilon_\theta$  is its approximation predicted by the model in the backward process. The goal is to only predict the added noise for removal instead of the entire image.

We based our model on ADM, where a U-Net [35]-based network is deployed for the denoising process. In addition to ADM, we introduce learnable object representations and a mask prediction subnetwork to process the layout information into unified global conditions for our model. Specifically, an object representation  $o^{\text{sty}} \in \mathbb{R}^{1 \times (d_e + d_z)}$  is a concatenation of a learnable categorical embedding  $c^{\text{emb}} \in \mathbb{R}^{1 \times d_e}$  and a randomly sampled  $z^{\text{sty}} \in \mathbb{R}^{1 \times d_z} \sim \mathcal{N}(0, 1)$  for controlling the object-specific details (i.e., style). The mask prediction subnetwork consists of a series of convolution layers, followed by a sigmoid transformation. It takes  $o^{\text{sty}}$  and predicts its initial object probabilistic mask  $M^0$ . Then, an input layout  $l$  is a collection of objects  $\{o_i^{\text{sty}}\}_{i=1}^N$  and their respective masks  $\{M_i^0\}_{i=1}^N$ , which we refer to as the global conditions for the DM.

As for the U-Net, we inherit the encoder part of ADM for noisy image encoding while designing novel modules for the decoder part to embed the global conditions. Particularly, we propose to use Layout Diffusion ResBlocks for the decoder part of our model, where we replace the Group

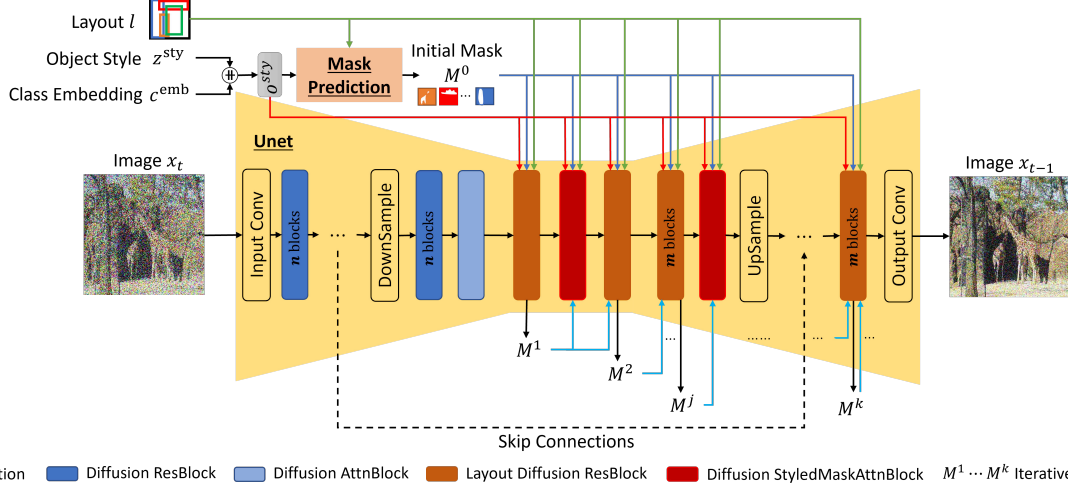


Figure 2. The architecture of the proposed STAY Diffusion. Through the guidance of the given layout, the learnable object representations  $o^{sty}$ , and their respective initial masks  $M^0$ , the model gradually turns a noisy image into a realistic real-world scene.

Normalization [48] layers with novel Edge-Aware Normalization (EA Norm) layers, and the updated object masks  $M^{j+1}$  are predicted at the end of the block (cf. Fig. 8(a) in Appendix A.1). Note that before passing to the next block, we follow the design in [41] to further refine  $M_i^{j+1}$  with  $M_i^{j+1} = (1 - \eta) \cdot M_i^0 + \eta \cdot M_i^{j+1}$ , where  $\eta$  is a learnable weight and  $i, j$  are the object and ResBlock indices, respectively. The proposed EA Norm is designed to fuse multiple objects smoothly and enable spatially-adaptive weight modulation. Additionally, a novel SM Attention is employed, allowing the model to only attend to relevant regions based on the given object masks.

### 3.2. Edge-Aware Normalization

Inspired by works in semantic image synthesis [30, 38, 46], the proposed EA Norm modulates the weight and bias of a normalization layer with a semantic map. Instead of using precisely labeled maps as input, where each pixel belongs to only one object, our EA Norm is designed to work with self-supervised object masks predicted from the layouts. Specifically, we noticed that methods that predict object masks independently, like [41] or ours, create false overlapping between objects (cf.  $B^j$  in Fig. 3). This results in multiple modulations being applied to one pixel. We hypothesize that ensuring the purity of these masks (i.e., the certainty of a pixel’s class) can significantly improve the quality of the assembled self-supervised map along with its generated image (cf. Sec. 4.6 for empirical results on this hypothesis). Thus, we design a new way to carefully utilize the self-supervised masks while limiting their overlap (see paragraph Edge-Aware Weighted Map below). Moreover, we propose to extend each predicted pixel with its object representation  $o_i^{sty}$  to improve the map’s expressiveness and the object controllability for guiding the generation. We il-

lustrate the whole workflow in Fig. 3 and formulate it as

$$\mathbf{feat}^{j+1} = \gamma^j \cdot \text{BatchNorm}(\mathbf{feat}^j) + \beta^j, \quad (4)$$

where  $\mathbf{feat}^j$  and  $\mathbf{feat}^{j+1}$  are the input and output features of EA Norm, respectively. The spatially aware weight  $\gamma^j$  and bias  $\beta^j$  are learned from the layout as follows.

**Edge-Aware Weighted Map.** To improve the clarity of object masks, we construct a pixel-level weighted semantic map from the object masks based on a given layout: we place the probabilistic object masks  $M^j$  to their bounding box locations and turn them into binary masks  $B^j$  by thresholding at 0. A **Non-Overlapping** semantic map  $m^{\text{non}}$  is computed such that for each pixel location only the object with the smallest mask in  $B^j$  remains activated (i.e., remains 1); otherwise, the pixel value is reset to 0. This is because we assume smaller objects have higher priority in claiming a pixel than larger ones. However, using the non-overlapping map alone may lead to unnatural boundaries in the generated images. Therefore, we also compute an **Edge-Aware** semantic map  $m^{\text{ea}}$ , which extends each object mask by one pixel at the borders using a mask dilation [47] operation. We associate the  $m^{\text{ea}}$  with learnable weights  $w$  for each object to fuse multiple objects in a given layout adaptively in the next step. The pixel-wise weighted map  $W_i^j$  for object  $i$  is then constructed as

$$\mathbf{W}_i^j = (m_i^{\text{non}} \odot M_i^j) + \alpha \cdot (m_i^{\text{ea}} \cdot w_i), \quad (5)$$

where  $\odot$  stands for the element-wise multiplication,  $i$  denotes the object index,  $w_i$  is the learnable edge weight to tune the intensity of each  $m^{\text{ea}}$ , and  $\alpha$  is a hyperparameter to balance between the two semantic maps. Finally, the object- and style-aware map  $\widehat{W}^j$  is computed as the sum of the object representations  $o^{sty}$  at each pixel location, weighted

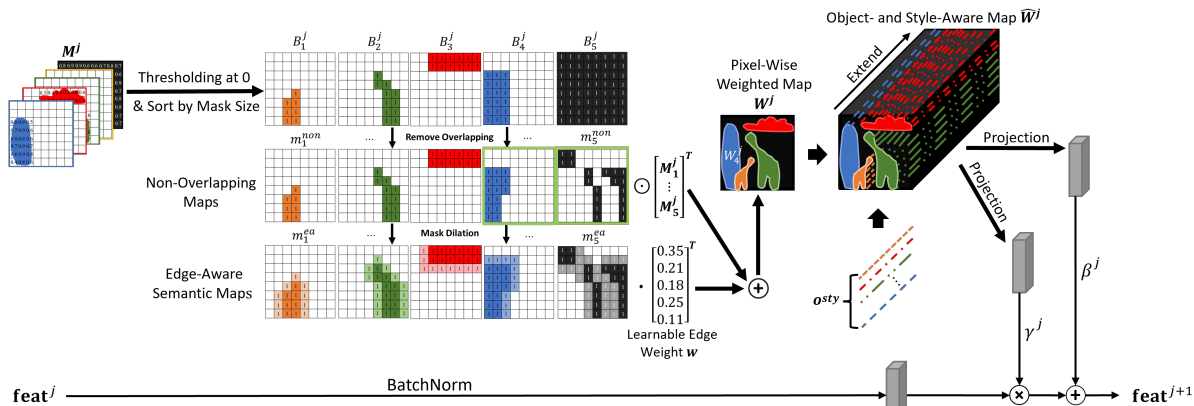


Figure 3. The workflow of the Edge-Aware Normalization, where object masks  $M^j$  are carefully assembled into a pixel-wise weighted map  $W^j$  and then extended by  $o^{\text{sty}}$  for computing the modulation parameters  $\gamma$  and  $\beta$ . Note that in  $m_4^{\text{non}}$  and  $m_5^{\text{non}}$  (highlighted in green), some pixels are removed (i.e., set to 0) due to overlapping with other smaller objects. See text for more details.

by the Edge-Aware Weighted Map  $W^j$ . The final spatially aware  $\gamma^j$  and  $\beta^j$  are then acquired via applying linear projection to  $\widehat{W}^j$ .

### 3.3. Styled-Mask Attention

To further strengthen the network’s attention on the given conditional information, we propose the SM Attention module, in which we replace the original self-attention by a novel mask attention layer (cf. Fig. 8(b) in Appendix A.1). A standard QKV attention [43] is defined as  $\text{Attention}(Q, K, V) = \text{softmax}(QK^T/\sqrt{d})V$ , where  $Q$ ,  $K$ , and  $V$  represent query, key, and value embeddings, respectively. Our SM Attention uses a cross-attention mechanism to stress the module to only pay attention to localized object regions according to a given layout. Specifically, we construct our query  $Q^j$  at layer  $j$  from the global conditions as follows: First, we compute a pixel-wise semantic map  $\widehat{m}^{\text{attn}} \in \mathbb{R}^{h \times w \times 1}$  with

$$\widehat{m}^{\text{attn}}(x, y) = \text{argmax}_i(\psi(M_i^j(x, y))), \quad (6)$$

where  $x, y$  are the map’s pixel coordinates,  $i$  is the object index,  $M^j$  are the object masks that are placed to their corresponding location and  $\psi(\cdot)$  denotes the operation to remove the overlapping pixels between objects. Then, we compute a more expressive semantic map  $m^{\text{attn}} \in \mathbb{R}^{h \times w \times (d_e + d_z)}$  based on  $\widehat{m}^{\text{attn}}$  by

$$m^{\text{attn}}(x, y) = o_{\widehat{m}^{\text{attn}}(x, y)}^{\text{sty}} \cdot M_{\widehat{m}^{\text{attn}}(x, y)}^j(x, y), \quad (7)$$

where  $o_{\widehat{m}^{\text{attn}}(x, y)}^{\text{sty}}$  is the object representation of the predicted class in  $\widehat{m}^{\text{attn}}$  and  $M_{\widehat{m}^{\text{attn}}(x, y)}^j(x, y)$  is its predicted probability. Finally, the  $Q$ ,  $K$  and  $V$  values for our mask attention layer are acquired by  $Q^j = \varphi_Q(m^{\text{attn}})$ ,  $K^j = \varphi_K(\text{feat}^j)$ ,  $V^j = \varphi_V(\text{feat}^j)$ , where  $\varphi_Q, \varphi_K, \varphi_V$  are linear projection layers.

### 3.4. Training and Sampling Schemes

Our STAY Diffusion is trained with two objective functions:  $\mathcal{L}_{\text{simple}}$  and  $\mathcal{L}_{\text{vlb}}$  as in ADM. Given an image  $x$  and a random timestep  $t \in \{0, 1, \dots, T\}$ , a noisy image  $\tilde{x}$  can be acquired through Eq. (1). The goal of our conditional DM is to reconstruct  $x$  by removing the added noise  $\epsilon$  at the timestep  $t$  under the guidance of a given layout  $l$ . This objective is referred to as  $\mathcal{L}_{\text{simple}}$ , which is formulated in Eq. (3). Additionally, we follow the proposal of Nicalol and Dhariwal [28] to not only model the noise but also parameterize the variance  $\Sigma_{\theta}(\tilde{x}_t, l, t)$ . The associated loss term  $\mathcal{L}_{\text{vlb}}$  is then defined as

$$\mathcal{L}_{\text{vlb}} = \text{KL}(q(\mathbf{x}_{t-1} | \mathbf{x}_t, \mathbf{x}_0) || p_{\theta}(\mathbf{x}_{t-1} | \mathbf{x}_t, \mathbf{l})) \quad (8)$$

and the overall objective is the weighted sum

$$\mathcal{L} = \mathcal{L}_{\text{simple}} + \lambda \cdot \mathcal{L}_{\text{vlb}}, \quad (9)$$

where  $\lambda$  is the non-negative trade-off hyperparameter to balance loss functions.

However, in contrast to ADM, we do not train an additional classifier to support the conditional sampling at inference time. Instead, we adapt the classifier-free guidance proposed in [14] to guide the sampling processes. The classifier-free guidance is accomplished by interpolating between the conditioned and unconditioned outputs of the model, where the unconditioned output can be acquired by replacing the given layout  $l$  with an empty layout  $l_{\emptyset} = \{(0, b_0)_i\}_{i=1}^N$ . At inference, the sampling procedure

$$\hat{\epsilon}_{\theta}(x_t, l, t) = \epsilon_{\theta}(x_t, l_{\emptyset}, t) + s \cdot (\epsilon_{\theta}(x_t, l, t) - \epsilon_{\theta}(x_t, l_{\emptyset}, t)) \quad (10)$$

is used, where  $\epsilon_{\theta}$  is the predicted noise from Eq. (3) and the non-negative scale  $s$  is a hyperparameter used to tune the strength of the guidance.

## 4. Experiments

In this section, we evaluate our STAY Diffusion on different benchmarks in terms of various metrics. First, we introduce the experimental settings including datasets, evaluation protocols and metrics. Second, we present the qualitative and quantitative comparisons between our method and previous SOTA methods. Third, we provide ablation studies to validate the effectiveness of the proposed EA Norm and SM Attention modules. Finally, we investigate the importance of the clarity of our self-supervised maps.

### 4.1. Datasets

Two benchmark datasets in L2I synthesis, **COCO-Stuff** [5] and **Visual Genome (VG)** [18], are used for our evaluations. The COCO-Stuff dataset contains pixel-level annotations for 80 things and 91 stuff classes. Following prior works [41, 56], we narrowed the image object count to 3–8 and excluded those with less than 2% coverage, yielding 112,680 training and 3,097 testing images across 171 categories. The VG dataset presents 108,077 images with dense annotation of objects, attributes, and relationships. We removed small objects and selected images of 3–30 bounding boxes as in [41, 56]. The refined dataset has 62,565 training and 5,096 testing images from 178 categories.

### 4.2. Evaluation Protocol & Metrics

We compared our results to previous L2I synthesis methods—LostGAN v2 [41], PLGAN [44], LAMA [21], TwFA [50], LayoutDiffuse [6], GLIGEN [20], and LayoutDM [56]—, and evaluated our self-supervised maps via semantic image synthesis benchmarks—ControlNet-v1.1 [52], FreestyleNet [49], PITI [45], and SDM [46]. All the following evaluations were done with models trained at resolution  $256 \times 256$  unless otherwise specified. See Appendix A for how we acquired images from other methods and more details of STAY Diffusion, including model architecture, training, and sampling hyperparameters.

Five popular metrics were used to evaluate the generated images from multiple aspects: we chose Fréchet inception distance (FID) [12] and Inception Score (IS) [37] for measuring the overall quality and visual appearance of the images. As for Diversity Score (DS), which estimates the diversity of the generated images, we follow other works [6, 41, 56] and adapt LPIPS [53] to compute the distance between two images from the same layout in the feature space. Also, we demonstrate the controllability of our method by calculating the Classification Score (CAS) [32], and the YoloScore (Yolo) [21]. The former uses the cropped generated images to train a ResNet-101 [10] classifier and test it on real images; the latter deploys a pre-trained YoloV4 [3] model to detect the 80 thing categories from the generated images. In other words, the model must

Table 1. Quantitative results on COCO-stuff and VG at resolution  $256 \times 256$ . The proposed STAY Diffusion outperforms LayoutDM in diversity, accuracy and controllability metrics while maintaining close quality performance.

Methods	Coco-Stuff				VG	
	FID ↓	DS ↑	CAS ↑	Yolo ↑	FID ↓	DS ↑
LostGAN v2 [41]	33.17	0.55±0.10	33.17	15.0	34.92	0.53±0.01
PLGAN [44]	30.67	0.52±0.10	29.15	13.6	-	-
LAMA [21]	33.00	0.48±0.12	9.97	20.4	38.51	0.54±0.10
TwFA [50]	23.78	0.43±0.13	20.09	23.9	18.57	0.50±0.10
LayoutDiffuse [6]	22.41	0.58±0.11	31.80	23.7	22.45	0.56±0.10
GLIGEN [20]	21.30	0.57±0.09	34.41	23.0	23.42	0.60±0.09
LayoutDM [56]	<b>15.74</b>	0.58±0.09	35.69	27.2	<b>15.26</b>	0.61±0.10
<b>Ours</b>	17.43	<b>0.59±0.09</b>	<b>37.18</b>	<b>29.5</b>	18.02	<b>0.65±0.08</b>

produce high-quality recognizable objects within the designated bounding boxes to reach a high CAS and YoloScore.

### 4.3. Qualitative Results

We present the qualitative comparisons of our STAY Diffusion to previous methods on COCO-Stuff in Fig. 4. Compared to other methods, STAY Diffusion produces more accurate high-quality images following the given layouts, while others like LayoutDiffuse produce artifacts despite using LTGM. Especially in scenes with complex object relationships, our method generates images with recognizable objects in the bounding boxes and has the least distortion. For example, in the first row of Fig. 4, only STAY Diffusion produced recognizable persons within the four bounding boxes labeled as “people”. Also, in the last row, our image faithfully presents the effect of fog while methods like LayoutDM failed. Moreover, the design of our EA Norm module allows STAY Diffusion to achieve fine-grained controllability over object appearance and predict self-supervised maps for the generated images. As shown in Fig. 5, STAY Diffusion can change the object’s attribute (i.e., the shape of the rock) by resampling its associated  $z^{\text{sty}}$  while conditioning on the same layout and input noise. This feature is especially appealing in domains like medical or industrial image augmentation, where a slight difference in object appearance (e.g., disease or defects) matters. On the other hand, LayoutDM does not offer such kind of control.

In Fig. 6, we present the self-supervised semantic maps learned in the EA Norm based on the provided layouts and illustrate the output diversity when the model is conditioned on the same layout but with different input noises (cf. Appendix C.2 for more results). Additionally, we showcase the interactivity of our approach in Appendix B.

### 4.4. Quantitative Results

We followed the protocol in [56] to form the evaluating sets by randomly sampling five images for each layout in COCO-stuff and one for VG for a fair comparison. The

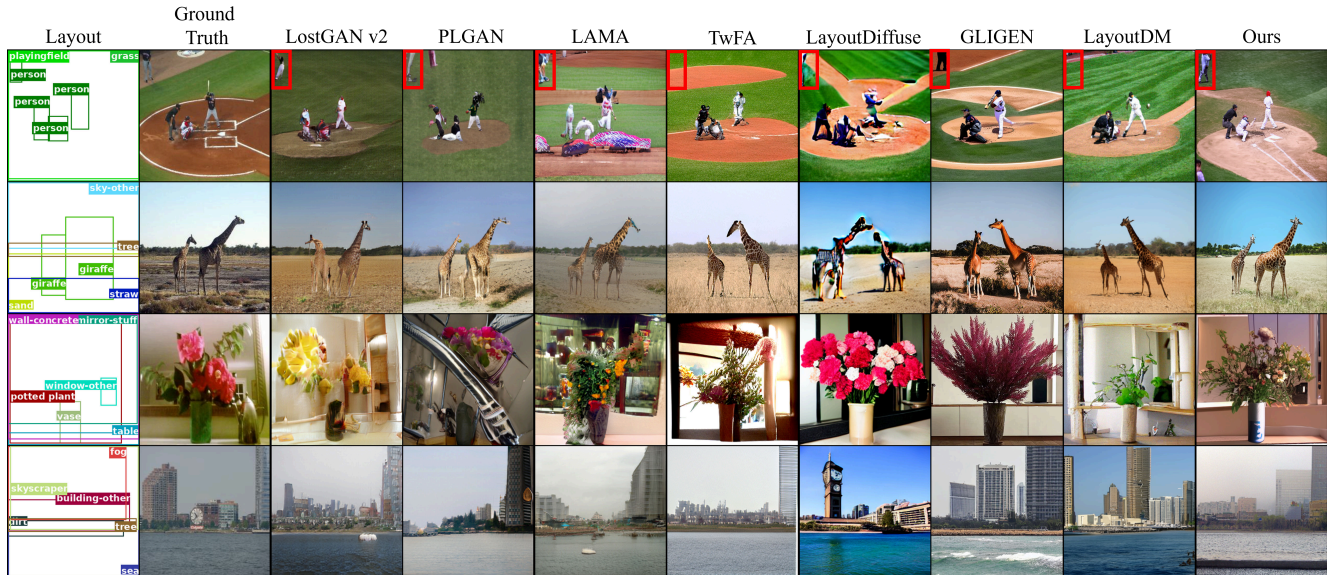


Figure 4. Qualitative comparison to the SOTA methods on COCO-stuff  $256 \times 256$ . STAY Diffusion shows better controllability and object recognizability over previous methods (e.g., the people on the playfield in the first row and the foggy effect in the last row). Zoom in for better view.

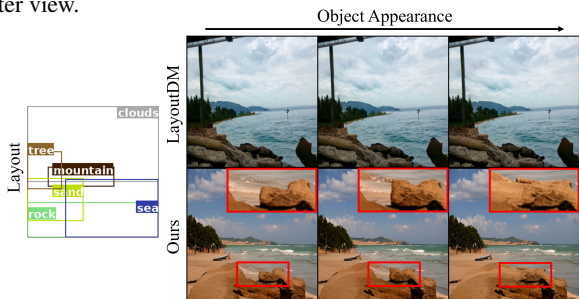


Figure 5. Given the same layout and input noise, STAY Diffusion can manipulate the appearance of an object (cf. the rock) by resampling its associated  $z^{\text{sty}}$  (Zoom in for better view).

quantitative results of our method in comparison to previous works are presented in Tab. 1. Due to the space limit, please see Appendix C.1 for the full tables. It can be observed that our STAY Diffusion surpasses non-DM methods in all metrics—notably, also the LTGM-based LayoutDiffuse and GLIGEN. As for the SOTA LayoutDM, our method outperforms in DS, CAS, and YoloScore while maintaining close performance in FID. We hypothesize that the differences in FID are due to the tighter constraints introduced by our proposed EA Norm and SM Attention, which heavily rely on the self-supervised maps. On the one hand, this allows superior accuracy and controllability in object generation as shown in Sec. 4.3. On the other hand, imperfections in the self-supervised maps can pose a hazard to the model and hinder the image fidelity. We further study the impact of the map’s quality in Sec. 4.6.

#### 4.5. Ablation Study

We conducted ablation experiments on different variants of our proposed method to understand the contributions of

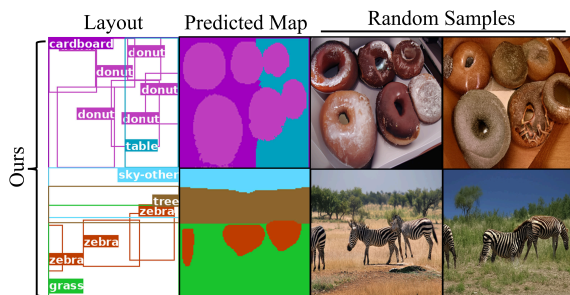


Figure 6. The self-supervised maps and their generated images. We randomly sampled two input noises to show the output diversity.

Table 2. Ablation study of the proposed EA Norm and SM Attention modules, where we trained the models on COCO-stuff  $128 \times 128$ .

	Norm	Attention	FID ↓	IS ↑	DS ↑	CAS ↑	Yolo ↑
(a)	ISLA [41]	Self	25.44	$13.36 \pm 0.72$	$0.56 \pm 0.1$	35.47	22.10
(b)	EA	Self	24.30	$14.68 \pm 0.56$	<b><math>0.59 \pm 0.1</math></b>	33.94	13.10
(c)	ISLA [41]	SM	24.60	$15.32 \pm 0.47$	$0.57 \pm 0.1$	34.26	20.90
(d)	EA	SM	<b>19.26</b>	<b><math>15.85 \pm 0.67</math></b>	$0.57 \pm 0.1$	<b>35.94</b>	<b>23.90</b>

each module. In Tab. 2, we present four settings. We considered the original ADM with a self-attention mechanism as the foundation and adapted ISLA Norm from LostGAN v2, which allows object overlapping, to take the layout as the condition. This case is referred to as (a) and is treated as the baseline for our method. Based on setting (a), we changed one component at a time in settings (b) and (c), where our EA Norm replaced the ISLA Norm in (b), and the self-attention was replaced by our SM Attention in (c), respectively. Finally, setting (d) stands for our full model. We evaluated all four variants with the evaluation metrics in

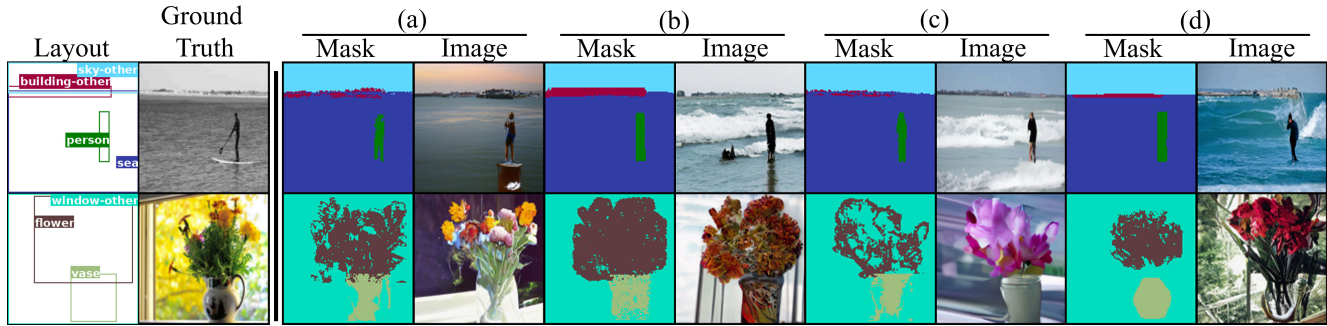


Figure 7. The generated images and their predicted self-supervised semantic maps from the ablated models in Tab. 2.

Sec. 4.2. The improvement in FID, IS, and DS shows that the use of EA Norm and SM Attention allows for higher generation quality and diversity. However, it can be observed that the performance of CAS and YoloScore fluctuated in settings (b) and (c). We hypothesized that it is due to the lack of global conditional information: the object awareness strengthened by the EA Norm was lost in the self-attention mechanism, and the ISLA Norm did not provide a strong localization signal for the SM Attention to follow. Our final model, which combines EA Norm with SM Attention, does not suffer from this issue. Moreover, it provides a better balance between diversity (i.e., DS) and controllability (i.e., CAS and YoloScore) compared to setting (a), suggesting the importance of the global condition.

Apart from the quantitative evaluation, we present the generated images and self-supervised semantic maps of all settings in Fig. 7. It can be seen that when the EA Norm is applied (i.e., in settings (b) and (d)), the predicted masks for objects are more integrated, demonstrating the effectiveness of our EA Norm. ISLA Norm (i.e., in settings (a) and (c)), on the other hand, produces masks with fragmented predictions. More results can be found in Appendix C.2.

#### 4.6. Mask Clarity

To investigate the importance of mask clarity as we hypothesized in Sec. 3.2, we provided three types of masks: the ground truth map (GT), the self-supervised map with overlapping objects from Tab. 2(a) (Base) and the self-supervised map from our full model (Ours) to the SOTA semantic synthesis methods for image generation. The evaluation results are shown in Tab. 3 (cf. Appendix C.3 for the full table and visual comparison). It can be observed that methods using GT maps show the best performance in all cases. However, if the perfectly labeled semantic maps are unavailable, our method and its self-supervised maps outperform all baselines in quality and controllability metrics. This showcases the superiority of our method in the case where only a bounding box layout is available. Moreover, we can observe a clear trend in method performance: GT map is better than Ours, which again is better than Base.

Table 3. Quantitative results of mask clarity on COCO-stuff 256  $\times$  256. When GT maps are absent, the images generated from the self-supervised maps of our full model (Ours) outperform other baseline methods in quality and controllability metrics, highlighting the importance of clear masks.

Methods	Mask	FID $\downarrow$	IS $\uparrow$	DS $\uparrow$	CAS $\uparrow$	Yolo $\uparrow$
ControlNet [52]	GT	32.24	24.80 $\pm$ 1.44	0.54 $\pm$ 0.08	22.43	25.6
FreestyleNet [49]	GT	14.80	30.06 $\pm$ 0.92	0.50 $\pm$ 0.09	36.67	42.9
ControlNet [52]	Base	64.29	17.47 $\pm$ 0.49	0.59 $\pm$ 0.09	9.36	4.1
FreestyleNet [49]	Base	37.21	20.40 $\pm$ 0.73	0.50 $\pm$ 0.09	21.54	12.9
ControlNet [52]	Ours	50.25	20.65 $\pm$ 0.93	0.60 $\pm$ 0.09	15.38	6.5
FreestyleNet [49]	Ours	32.95	22.59 $\pm$ 0.66	0.56 $\pm$ 0.10	26.52	13.8
PITI [45]	Ours	37.41	17.24 $\pm$ 0.91	0.53 $\pm$ 0.13	18.63	12.0
SDM [46]	Ours	35.53	17.70 $\pm$ 0.72	<b>0.69<math>\pm</math>0.19</b>	22.69	13.5
<b>Ours</b>	Ours	<b>17.43</b>	<b>26.08<math>\pm</math>0.76</b>	0.59 $\pm$ 0.09	<b>37.18</b>	<b>29.5</b>

This indicates that further improving self-supervised maps' quality (e.g., through increasing mask clarity) is a promising way to enhance generation quality. We leave this for future work.

## 5. Conclusion

In this paper, we introduce STyled LAYout Diffusion (STAY Diffusion), a diffusion-based model with novel designed normalization and attention modules for layout-to-image synthesis. With the newly proposed Edge-Aware Normalization module, our diffusion model learns a latent representation for each bounding box object in a layout and predicts a self-supervised map for more precise condition guidance. In addition, we proposed the Styled-Mask Attention to capturing the object's relationship based on the learned object representations and maps from the normalization module, forming consistent global conditions through the model. These two critical designs allow our STAY Diffusion to perform more fine-grained object control compared to previous methods. Extensive results on the challenging COCO-stuff and Visual Genome dataset show that STAY Diffusion can not only produce high-quality images but also outperform previous state-of-the-art regarding generation diversity, accuracy, and controllability.



## References

- [1] Oron Ashual and Lior Wolf. Specifying object attributes and relations in interactive scene generation. *Proceedings of the IEEE International Conference on Computer Vision (ICCV)*, pages 4560–4568, 2019. 1
- [2] Omri Avrahami, Dani Lischinski, and Ohad Fried. Blended diffusion for text-driven editing of natural images. In *Proceedings of the IEEE/CVF Conference on Computer Vision and Pattern Recognition (CVPR)*, pages 18208–18218, June 2022. 2
- [3] Alexey Bochkovskiy, Chien-Yao Wang, and Hong-Yuan Mark Liao. Yolov4: Optimal speed and accuracy of object detection. *arXiv preprint arXiv:2004.10934*, 2020. 6
- [4] Andrew Brock, Jeff Donahue, and Karen Simonyan. Large scale gan training for high fidelity natural image synthesis. *arXiv preprint arXiv:1809.11096*, 2018. 2
- [5] Holger Caesar, Jasper Uijlings, and Vittorio Ferrari. Cocomstuff: Thing and stuff classes in context. In *Proceedings of the IEEE/CVF Conference on Computer Vision and Pattern Recognition (CVPR)*, pages 1209–1218, 2018. 2, 6
- [6] Jiaxin Cheng, Xiao Liang, Xingjian Shi, Tong He, Tianjun Xiao, and Mu Li. Layoutdiffuse: Adapting foundational diffusion models for layout-to-image generation. *arXiv, abs/2302.08908*, 2023. 1, 3, 6, 14, 17
- [7] Prafulla Dhariwal and Alexander Nichol. Diffusion models beat gans on image synthesis. *Advances in Neural Information Processing Systems (NeurIPS)*, 34:8780–8794, 2021. 1, 2
- [8] Patrick Esser, Robin Rombach, and Björn Ommer. Taming transformers for high-resolution image synthesis. *Proceedings of the IEEE/CVF Conference on Computer Vision and Pattern Recognition (CVPR)*, pages 12868–12878, 2020. 3
- [9] Ian Goodfellow, Jean Pouget-Abadie, Mehdi Mirza, Bing Xu, David Warde-Farley, Sherjil Ozair, Aaron Courville, and Yoshua Bengio. Generative adversarial nets. *Advances in Neural Information Processing Systems (NeurIPS)*, 27, 2014. 2
- [10] Kaiming He, Xiangyu Zhang, Shaoqing Ren, and Jian Sun. Deep residual learning for image recognition. In *Proceedings of the IEEE/CVF Conference on Computer Vision and Pattern Recognition (CVPR)*, pages 770–778, 2016. 6
- [11] Sen He, Wentong Liao, Michael Ying Yang, Yongxin Yang, Yi-Zhe Song, Bodo Rosenhahn, and Tao Xiang. Context-aware layout to image generation with enhanced object appearance. *Proceedings of the IEEE/CVF Conference on Computer Vision and Pattern Recognition (CVPR)*, pages 15044–15053, 2021. 2, 3
- [12] Martin Heusel, Hubert Ramsauer, Thomas Unterthiner, Bernhard Nessler, Günter Klambauer, and Sepp Hochreiter. Gans trained by a two time-scale update rule converge to a nash equilibrium. *arXiv, abs/1706.08500*, 2017. 6
- [13] Jonathan Ho, Ajay Jain, and Pieter Abbeel. Denoising diffusion probabilistic models. *Advances in Neural Information Processing Systems (NeurIPS)*, 33:6840–6851, 2020. 1, 2, 3
- [14] Jonathan Ho and Tim Salimans. Classifier-free diffusion guidance. *arXiv preprint arXiv:2207.12598*, 2022. 2, 5
- [15] Xun Huang and Serge J. Belongie. Arbitrary style transfer in real-time with adaptive instance normalization. *Proceedings of the IEEE International Conference on Computer Vision (ICCV)*, pages 1510–1519, 2017. 2
- [16] Manuel Jahn, Robin Rombach, and Björn Ommer. High-resolution complex scene synthesis with transformers. *arXiv, abs/2105.06458*, 2021. 3
- [17] Tero Karras, Samuli Laine, Miika Aittala, Janne Hellsten, Jaakko Lehtinen, and Timo Aila. Analyzing and improving the image quality of StyleGAN. In *Proceedings of the IEEE/CVF Conference on Computer Vision and Pattern Recognition (CVPR)*, 2020. 1, 2
- [18] Ranjay Krishna, Yuke Zhu, Oliver Groth, Justin Johnson, Kenji Hata, Joshua Kravitz, Stephanie Chen, Yannis Kalantidis, Li-Jia Li, David A. Shamma, Michael S. Bernstein, and Li Fei-Fei. Visual genome: Connecting language and vision using crowdsourced dense image annotations. *International Journal of Computer Vision*, 123:32 – 73, 2016. 2, 6
- [19] Haoying Li, Yifan Yang, Meng Chang, Shiqi Chen, Huajun Feng, Zhihai Xu, Qi Li, and Yueting Chen. Srdiff: Single image super-resolution with diffusion probabilistic models. *Neurocomputing*, 479:47–59, 2022. 2
- [20] Yuheng Li, Haotian Liu, Qingyang Wu, Fangzhou Mu, Jianwei Yang, Jianfeng Gao, Chunyuan Li, and Yong Jae Lee. Gligen: Open-set grounded text-to-image generation. *Proceedings of the IEEE/CVF Conference on Computer Vision and Pattern Recognition (CVPR)*, pages 22511–22521, 2023. 1, 3, 6, 14, 17
- [21] Zejian Li, Jingyu Wu, Immanuel Koh, Yongchuan Tang, and Lingyun Sun. Image synthesis from layout with locality-aware mask adaption. In *Proceedings of the IEEE International Conference on Computer Vision (ICCV)*, pages 13799–13808, 2021. 2, 3, 6, 14, 15, 17
- [22] Andreas Lugmayr, Martin Danelljan, Andrés Romero, Fisher Yu, Radu Timofte, and Luc Van Gool. Repaint: Inpainting using denoising diffusion probabilistic models. *Proceedings of the IEEE/CVF Conference on Computer Vision and Pattern Recognition (CVPR)*, pages 11451–11461, 2022. 2
- [23] Mehdi Mirza and Simon Osindero. Conditional generative adversarial nets. *arXiv, abs/1411.1784*, 2014. 2
- [24] Pamela Mishkin, Lama Ahmad, Miles Brundage, Gretchen Krueger, and Girish Sastry. Dall-e 2 preview - risks and limitations. 2022. 2
- [25] Takeru Miyato and Masanori Koyama. cgans with projection discriminator. *arXiv, abs/1802.05637*, 2018. 2
- [26] Chong Mou, Xintao Wang, Liangbin Xie, Yanze Wu, Jian Zhang, Zhongang Qi, and Ying Shan. T2i-adapter: Learning adapters to dig out more controllable ability for text-to-image diffusion models. In *Proceedings of the AAAI Conference on Artificial Intelligence (AAAI)*, volume 38, pages 4296–4304, 2024. 2
- [27] Alex Nichol, Prafulla Dhariwal, Aditya Ramesh, Pranav Shyam, Pamela Mishkin, Bob McGrew, Ilya Sutskever, and Mark Chen. Glide: Towards photorealistic image generation and editing with text-guided diffusion models. In *Proceedings of the International Conference on Machine Learning (ICML)*, 2021. 2

- [28] Alexander Quinn Nichol and Prafulla Dhariwal. Improved denoising diffusion probabilistic models. In *Proceedings of the International Conference on Machine Learning (ICML)*, pages 8162–8171. PMLR, 2021. 1, 2, 5
- [29] Augustus Odena, Christopher Olah, and Jonathon Shlens. Conditional image synthesis with auxiliary classifier gans. In *Proceedings of the International Conference on Machine Learning (ICML)*, 2016. 2
- [30] Taesung Park, Ming-Yu Liu, Ting-Chun Wang, and Jun-Yan Zhu. Semantic image synthesis with spatially-adaptive normalization. In *Proceedings of the IEEE/CVF Conference on Computer Vision and Pattern Recognition (CVPR)*, 2019. 2, 4
- [31] Alec Radford, Jong Wook Kim, Chris Hallacy, Aditya Ramesh, Gabriel Goh, Sandhini Agarwal, Girish Sastry, Amanda Askell, Pamela Mishkin, Jack Clark, Gretchen Krueger, and Ilya Sutskever. Learning transferable visual models from natural language supervision. In *Proceedings of the International Conference on Machine Learning (ICML)*, 2021. 2
- [32] Suman Ravuri and Oriol Vinyals. Classification accuracy score for conditional generative models. *Advances in Neural Information Processing Systems (NeurIPS)*, 32, 2019. 6
- [33] Scott E. Reed, Zeynep Akata, Xinchen Yan, Lajanugen Logeswaran, Bernt Schiele, and Honglak Lee. Generative adversarial text to image synthesis. In *Proceedings of the International Conference on Machine Learning (ICML)*, 2016. 2
- [34] Robin Rombach, Andreas Blattmann, Dominik Lorenz, Patrick Esser, and Björn Ommer. High-resolution image synthesis with latent diffusion models, 2021. 1, 2, 3, 14
- [35] Olaf Ronneberger, Philipp Fischer, and Thomas Brox. U-net: Convolutional networks for biomedical image segmentation. In *Medical Image Computing and Computer-Assisted Intervention–MICCAI 2015: 18th International Conference, Munich, Germany, October 5–9, 2015, Proceedings, Part III 18*, pages 234–241. Springer, 2015. 3
- [36] Chitwan Saharia, William Chan, Saurabh Saxena, Lala Li, Jay Whang, Emily L Denton, Kamyar Ghasemipour, Raphael Gontijo Lopes, Burcu Karagol Ayan, Tim Salimans, et al. Photorealistic text-to-image diffusion models with deep language understanding. *Advances in Neural Information Processing Systems (NeurIPS)*, 35:36479–36494, 2022. 2
- [37] Tim Salimans, Ian Goodfellow, Wojciech Zaremba, Vicki Cheung, Alec Radford, and Xi Chen. Improved techniques for training gans. *Advances in Neural Information Processing Systems (NeurIPS)*, 29, 2016. 6
- [38] Edgar Schönfeld, Vadim Sushko, Dan Zhang, Juergen Gall, Bernt Schiele, and Anna Khoreva. You only need adversarial supervision for semantic image synthesis. In *Proceedings of the International Conference on Learning Representations (ICLR)*, 2021. 2, 4
- [39] Jiaming Song, Chenlin Meng, and Stefano Ermon. Denoising diffusion implicit models. *arXiv preprint arXiv:2010.02502*, 2020. 1, 2
- [40] Yang Song and Stefano Ermon. Generative modeling by estimating gradients of the data distribution. *Advances in Neural Information Processing Systems (NeurIPS)*, 32, 2019. 1
- [41] Wei Sun and Tianfu Wu. Image synthesis from reconfigurable layout and style. In *Proceedings of the IEEE International Conference on Computer Vision (ICCV)*, pages 10531–10540, 2019. 1, 2, 3, 4, 6, 7, 14, 17
- [42] Arash Vahdat, Karsten Kreis, and Jan Kautz. Score-based generative modeling in latent space. In *Advances in Neural Information Processing Systems (NeurIPS)*, 2021. 1
- [43] Ashish Vaswani, Noam Shazeer, Niki Parmar, Jakob Uszkoreit, Llion Jones, Aidan N Gomez, Łukasz Kaiser, and Illia Polosukhin. Attention is all you need. *Advances in Neural Information Processing Systems (NeurIPS)*, 30, 2017. 5
- [44] Bo Wang, Tao Wu, Minfeng Zhu, and Peng Du. Interactive image synthesis with panoptic layout generation. *Proceedings of the IEEE/CVF Conference on Computer Vision and Pattern Recognition (CVPR)*, pages 7773–7782, 2022. 2, 3, 6, 14, 17
- [45] Tengfei Wang, Ting Zhang, Bo Zhang, Hao Ouyang, Dong Chen, Qifeng Chen, and Fang Wen. Pretraining is all you need for image-to-image translation. *arXiv preprint arXiv:2205.12952*, 2022. 2, 6, 8, 14, 17
- [46] Weilun Wang, Jianmin Bao, Wen gang Zhou, Dongdong Chen, Dong Chen, Lu Yuan, and Houqiang Li. Semantic image synthesis via diffusion models. *arXiv*, abs/2207.00050, 2022. 2, 4, 6, 8, 14, 17
- [47] Wikipedia contributors. Dilation (morphology) — Wikipedia, the free encyclopedia, 2023. [Online; accessed 17-June-2024]. 4
- [48] Yuxin Wu and Kaiming He. Group normalization. In *Proceedings of the European Conference on Computer Vision (ECCV)*, pages 3–19, 2018. 4, 14
- [49] Han Xue, Zhiwu Huang, Qianru Sun, Li Song, and Wenjun Zhang. Freestyle layout-to-image synthesis. In *Proceedings of the IEEE/CVF Conference on Computer Vision and Pattern Recognition (CVPR)*, pages 14256–14266, 2023. 2, 6, 8, 14, 17
- [50] Zuopeng Yang, Daqing Liu, Chaoyue Wang, J. Yang, and Dacheng Tao. Modeling image composition for complex scene generation. *Proceedings of the IEEE/CVF Conference on Computer Vision and Pattern Recognition (CVPR)*, pages 7754–7763, 2022. 1, 3, 6, 14, 17
- [51] Han Zhang, Ian Goodfellow, Dimitris Metaxas, and Augustus Odena. Self-attention generative adversarial networks. In *Proceedings of the International Conference on Machine Learning (ICML)*, pages 7354–7363. PMLR, 2019. 2
- [52] Lvmin Zhang, Anyi Rao, and Maneesh Agrawala. Adding conditional control to text-to-image diffusion models. In *Proceedings of the IEEE International Conference on Computer Vision (ICCV)*, pages 3836–3847, 2023. 2, 6, 8, 14, 17
- [53] Richard Zhang, Phillip Isola, Alexei A Efros, Eli Shechtman, and Oliver Wang. The unreasonable effectiveness of deep features as a perceptual metric. In *Proceedings of the IEEE/CVF Conference on Computer Vision and Pattern Recognition (CVPR)*, 2018. 6
- [54] Bo Zhao, Lili Meng, Weidong Yin, and Leonid Sigal. Image generation from layout. *Proceedings of the IEEE/CVF Conference on Computer Vision and Pattern Recognition (CVPR)*, pages 8576–8585, 2018. 1, 3

- [55] Bo Zhao, Lili Meng, Weidong Yin, and Leonid Sigal. Image generation from layout. In *Proceedings of the IEEE/CVF Conference on Computer Vision and Pattern Recognition (CVPR)*, 2019. [1](#)
- [56] Guangcong Zheng, Xianpan Zhou, Xuewei Li, Zhongang Qi, Ying Shan, and Xi Li. Layoutdiffusion: Controllable diffusion model for layout-to-image generation. In *Proceedings of the IEEE/CVF Conference on Computer Vision and Pattern Recognition (CVPR)*, pages 22490–22499, June 2023. [1](#), [3](#), [6](#), [14](#), [17](#)

## References

- [1] Oron Ashual and Lior Wolf. Specifying object attributes and relations in interactive scene generation. *Proceedings of the IEEE International Conference on Computer Vision (ICCV)*, pages 4560–4568, 2019. [1](#)
- [2] Omri Avrahami, Dani Lischinski, and Ohad Fried. Blended diffusion for text-driven editing of natural images. In *Proceedings of the IEEE/CVF Conference on Computer Vision and Pattern Recognition (CVPR)*, pages 18208–18218, June 2022. [2](#)
- [3] Alexey Bochkovskiy, Chien-Yao Wang, and Hong-Yuan Mark Liao. Yolov4: Optimal speed and accuracy of object detection. *arXiv preprint arXiv:2004.10934*, 2020. [6](#)
- [4] Andrew Brock, Jeff Donahue, and Karen Simonyan. Large scale gan training for high fidelity natural image synthesis. *arXiv preprint arXiv:1809.11096*, 2018. [2](#)
- [5] Holger Caesar, Jasper Uijlings, and Vittorio Ferrari. Coco-stuff: Thing and stuff classes in context. In *Proceedings of the IEEE/CVF Conference on Computer Vision and Pattern Recognition (CVPR)*, pages 1209–1218, 2018. [2](#), [6](#)
- [6] Jiaxin Cheng, Xiao Liang, Xingjian Shi, Tong He, Tianjun Xiao, and Mu Li. Layoutdiffuse: Adapting foundational diffusion models for layout-to-image generation. *arXiv*, abs/2302.08908, 2023. [1](#), [3](#), [6](#), [14](#), [17](#)
- [7] Prafulla Dhariwal and Alexander Nichol. Diffusion models beat gans on image synthesis. *Advances in Neural Information Processing Systems (NeurIPS)*, 34:8780–8794, 2021. [1](#), [2](#)
- [8] Patrick Esser, Robin Rombach, and Björn Ommer. Taming transformers for high-resolution image synthesis. *Proceedings of the IEEE/CVF Conference on Computer Vision and Pattern Recognition (CVPR)*, pages 12868–12878, 2020. [3](#)
- [9] Ian Goodfellow, Jean Pouget-Abadie, Mehdi Mirza, Bing Xu, David Warde-Farley, Sherjil Ozair, Aaron Courville, and Yoshua Bengio. Generative adversarial nets. *Advances in Neural Information Processing Systems (NeurIPS)*, 27, 2014. [2](#)
- [10] Kaiming He, Xiangyu Zhang, Shaoqing Ren, and Jian Sun. Deep residual learning for image recognition. In *Proceedings of the IEEE/CVF Conference on Computer Vision and Pattern Recognition (CVPR)*, pages 770–778, 2016. [6](#)
- [11] Sen He, Wentong Liao, Michael Ying Yang, Yongxin Yang, Yi-Zhe Song, Bodo Rosenhahn, and Tao Xiang. Context-aware layout to image generation with enhanced object appearance. *Proceedings of the IEEE/CVF Conference on Computer Vision and Pattern Recognition (CVPR)*, pages 15044–15053, 2021. [2](#), [3](#)
- [12] Martin Heusel, Hubert Ramsauer, Thomas Unterthiner, Bernhard Nessler, Günter Klambauer, and Sepp Hochreiter. Gans trained by a two time-scale update rule converge to a nash equilibrium. *arXiv*, abs/1706.08500, 2017. [6](#)
- [13] Jonathan Ho, Ajay Jain, and Pieter Abbeel. Denoising diffusion probabilistic models. *Advances in Neural Information Processing Systems (NeurIPS)*, 33:6840–6851, 2020. [1](#), [2](#), [3](#)
- [14] Jonathan Ho and Tim Salimans. Classifier-free diffusion guidance. *arXiv preprint arXiv:2207.12598*, 2022. [2](#), [5](#)
- [15] Xun Huang and Serge J. Belongie. Arbitrary style transfer in real-time with adaptive instance normalization. *Proceedings of the IEEE International Conference on Computer Vision (ICCV)*, pages 1510–1519, 2017. [2](#)
- [16] Manuel Jahn, Robin Rombach, and Björn Ommer. High-resolution complex scene synthesis with transformers. *arXiv*, abs/2105.06458, 2021. [3](#)
- [17] Tero Karras, Samuli Laine, Miika Aittala, Janne Hellsten, Jaakko Lehtinen, and Timo Aila. Analyzing and improving the image quality of StyleGAN. In *Proceedings of the IEEE/CVF Conference on Computer Vision and Pattern Recognition (CVPR)*, 2020. [1](#), [2](#)
- [18] Ranjay Krishna, Yuke Zhu, Oliver Groth, Justin Johnson, Kenji Hata, Joshua Kravitz, Stephanie Chen, Yannis Kalantidis, Li-Jia Li, David A. Shamma, Michael S. Bernstein, and Li Fei-Fei. Visual genome: Connecting language and vision using crowdsourced dense image annotations. *International Journal of Computer Vision*, 123:32–73, 2016. [2](#), [6](#)
- [19] Haoying Li, Yifan Yang, Meng Chang, Shiqi Chen, Huajun Feng, Zhihai Xu, Qi Li, and Yueting Chen. Srdiff: Single image super-resolution with diffusion probabilistic models. *Neurocomputing*, 479:47–59, 2022. [2](#)
- [20] Yuheng Li, Haotian Liu, Qingyang Wu, Fangzhou Mu, Jianwei Yang, Jianfeng Gao, Chunyuan Li, and Yong Jae Lee. Gligen: Open-set grounded text-to-image generation. *Proceedings of the IEEE/CVF Conference on Computer Vision and Pattern Recognition (CVPR)*, pages 22511–22521, 2023. [1](#), [3](#), [6](#), [14](#), [17](#)
- [21] Zejian Li, Jingyu Wu, Immanuel Koh, Yongchuan Tang, and Lingyun Sun. Image synthesis from layout with locality-aware mask adaption. In *Proceedings of the IEEE International Conference on Computer Vision (ICCV)*, pages 13799–13808, 2021. [2](#), [3](#), [6](#), [14](#), [15](#), [17](#)
- [22] Andreas Lugmayr, Martin Danelljan, Andrés Romero, Fisher Yu, Radu Timofte, and Luc Van Gool. Repaint: Inpainting using denoising diffusion probabilistic models. *Proceedings of the IEEE/CVF Conference on Computer Vision and Pattern Recognition (CVPR)*, pages 11451–11461, 2022. [2](#)
- [23] Mehdi Mirza and Simon Osindero. Conditional generative adversarial nets. *arXiv*, abs/1411.1784, 2014. [2](#)
- [24] Pamela Mishkin, Lama Ahmad, Miles Brundage, Gretchen Krueger, and Girish Sastry. Dall-e 2 preview - risks and limitations. 2022. [2](#)
- [25] Takeru Miyato and Masanori Koyama. cgans with projection discriminator. *arXiv*, abs/1802.05637, 2018. [2](#)

- [26] Chong Mou, Xintao Wang, Liangbin Xie, Yanze Wu, Jian Zhang, Zhongang Qi, and Ying Shan. T2i-adapter: Learning adapters to dig out more controllable ability for text-to-image diffusion models. In *Proceedings of the AAAI Conference on Artificial Intelligence (AAAI)*, volume 38, pages 4296–4304, 2024. 2
- [27] Alex Nichol, Prafulla Dhariwal, Aditya Ramesh, Pranav Shyam, Pamela Mishkin, Bob McGrew, Ilya Sutskever, and Mark Chen. Glide: Towards photorealistic image generation and editing with text-guided diffusion models. In *Proceedings of the International Conference on Machine Learning (ICML)*, 2021. 2
- [28] Alexander Quinn Nichol and Prafulla Dhariwal. Improved denoising diffusion probabilistic models. In *Proceedings of the International Conference on Machine Learning (ICML)*, pages 8162–8171. PMLR, 2021. 1, 2, 5
- [29] Augustus Odena, Christopher Olah, and Jonathon Shlens. Conditional image synthesis with auxiliary classifier gans. In *Proceedings of the International Conference on Machine Learning (ICML)*, 2016. 2
- [30] Taesung Park, Ming-Yu Liu, Ting-Chun Wang, and Jun-Yan Zhu. Semantic image synthesis with spatially-adaptive normalization. In *Proceedings of the IEEE/CVF Conference on Computer Vision and Pattern Recognition (CVPR)*, 2019. 2, 4
- [31] Alec Radford, Jong Wook Kim, Chris Hallacy, Aditya Ramesh, Gabriel Goh, Sandhini Agarwal, Girish Sastry, Amanda Askell, Pamela Mishkin, Jack Clark, Gretchen Krueger, and Ilya Sutskever. Learning transferable visual models from natural language supervision. In *Proceedings of the International Conference on Machine Learning (ICML)*, 2021. 2
- [32] Suman Ravuri and Oriol Vinyals. Classification accuracy score for conditional generative models. *Advances in Neural Information Processing Systems (NeurIPS)*, 32, 2019. 6
- [33] Scott E. Reed, Zeynep Akata, Xinchun Yan, Lajanugen Logeswaran, Bernt Schiele, and Honglak Lee. Generative adversarial text to image synthesis. In *Proceedings of the International Conference on Machine Learning (ICML)*, 2016. 2
- [34] Robin Rombach, Andreas Blattmann, Dominik Lorenz, Patrick Esser, and Björn Ommer. High-resolution image synthesis with latent diffusion models, 2021. 1, 2, 3, 14
- [35] Olaf Ronneberger, Philipp Fischer, and Thomas Brox. U-net: Convolutional networks for biomedical image segmentation. In *Medical Image Computing and Computer-Assisted Intervention—MICCAI 2015: 18th International Conference, Munich, Germany, October 5-9, 2015, Proceedings, Part III 18*, pages 234–241. Springer, 2015. 3
- [36] Chitwan Saharia, William Chan, Saurabh Saxena, Lala Li, Jay Whang, Emily L Denton, Kamyar Ghasemipour, Raphael Gontijo Lopes, Burcu Karagol Ayan, Tim Salimans, et al. Photorealistic text-to-image diffusion models with deep language understanding. *Advances in Neural Information Processing Systems (NeurIPS)*, 35:36479–36494, 2022. 2
- [37] Tim Salimans, Ian Goodfellow, Wojciech Zaremba, Vicki Cheung, Alec Radford, and Xi Chen. Improved techniques for training gans. *Advances in Neural Information Processing Systems (NeurIPS)*, 29, 2016. 6
- [38] Edgar Schönfeld, Vadim Sushko, Dan Zhang, Juergen Gall, Bernt Schiele, and Anna Khoreva. You only need adversarial supervision for semantic image synthesis. In *Proceedings of the International Conference on Learning Representations (ICLR)*, 2021. 2, 4
- [39] Jiaming Song, Chenlin Meng, and Stefano Ermon. Denoising diffusion implicit models. *arXiv preprint arXiv:2010.02502*, 2020. 1, 2
- [40] Yang Song and Stefano Ermon. Generative modeling by estimating gradients of the data distribution. *Advances in Neural Information Processing Systems (NeurIPS)*, 32, 2019. 1
- [41] Wei Sun and Tianfu Wu. Image synthesis from reconfigurable layout and style. In *Proceedings of the IEEE International Conference on Computer Vision (ICCV)*, pages 10531–10540, 2019. 1, 2, 3, 4, 6, 7, 14, 17
- [42] Arash Vahdat, Karsten Kreis, and Jan Kautz. Score-based generative modeling in latent space. In *Advances in Neural Information Processing Systems (NeurIPS)*, 2021. 1
- [43] Ashish Vaswani, Noam Shazeer, Niki Parmar, Jakob Uszkoreit, Llion Jones, Aidan N Gomez, Łukasz Kaiser, and Illia Polosukhin. Attention is all you need. *Advances in Neural Information Processing Systems (NeurIPS)*, 30, 2017. 5
- [44] Bo Wang, Tao Wu, Minfeng Zhu, and Peng Du. Interactive image synthesis with panoptic layout generation. *Proceedings of the IEEE/CVF Conference on Computer Vision and Pattern Recognition (CVPR)*, pages 7773–7782, 2022. 2, 3, 6, 14, 17
- [45] Tengfei Wang, Ting Zhang, Bo Zhang, Hao Ouyang, Dong Chen, Qifeng Chen, and Fang Wen. Pretraining is all you need for image-to-image translation. *arXiv preprint arXiv:2205.12952*, 2022. 2, 6, 8, 14, 17
- [46] Weilun Wang, Jianmin Bao, Wen gang Zhou, Dongdong Chen, Dong Chen, Lu Yuan, and Houqiang Li. Semantic image synthesis via diffusion models. *arXiv*, abs/2207.00050, 2022. 2, 4, 6, 8, 14, 17
- [47] Wikipedia contributors. Dilation (morphology) — Wikipedia, the free encyclopedia, 2023. [Online; accessed 17-June-2024]. 4
- [48] Yuxin Wu and Kaiming He. Group normalization. In *Proceedings of the European Conference on Computer Vision (ECCV)*, pages 3–19, 2018. 4, 14
- [49] Han Xue, Zhiwu Huang, Qianru Sun, Li Song, and Wenjun Zhang. Freestyle layout-to-image synthesis. In *Proceedings of the IEEE/CVF Conference on Computer Vision and Pattern Recognition (CVPR)*, pages 14256–14266, 2023. 2, 6, 8, 14, 17
- [50] Zuopeng Yang, Daqing Liu, Chaoyue Wang, J. Yang, and Dacheng Tao. Modeling image composition for complex scene generation. *Proceedings of the IEEE/CVF Conference on Computer Vision and Pattern Recognition (CVPR)*, pages 7754–7763, 2022. 1, 3, 6, 14, 17
- [51] Han Zhang, Ian Goodfellow, Dimitris Metaxas, and Augustus Odena. Self-attention generative adversarial networks. In *Proceedings of the International Conference on Machine Learning (ICML)*, pages 7354–7363. PMLR, 2019. 2

- [52] Lvmin Zhang, Anyi Rao, and Maneesh Agrawala. Adding conditional control to text-to-image diffusion models. In *Proceedings of the IEEE International Conference on Computer Vision (ICCV)*, pages 3836–3847, 2023. [2](#), [6](#), [8](#), [14](#), [17](#)
- [53] Richard Zhang, Phillip Isola, Alexei A Efros, Eli Shechtman, and Oliver Wang. The unreasonable effectiveness of deep features as a perceptual metric. In *Proceedings of the IEEE/CVF Conference on Computer Vision and Pattern Recognition (CVPR)*, 2018. [6](#)
- [54] Bo Zhao, Lili Meng, Weidong Yin, and Leonid Sigal. Image generation from layout. *Proceedings of the IEEE/CVF Conference on Computer Vision and Pattern Recognition (CVPR)*, pages 8576–8585, 2018. [1](#), [3](#)
- [55] Bo Zhao, Lili Meng, Weidong Yin, and Leonid Sigal. Image generation from layout. In *Proceedings of the IEEE/CVF Conference on Computer Vision and Pattern Recognition (CVPR)*, 2019. [1](#)
- [56] Guangcong Zheng, Xianpan Zhou, Xuwei Li, Zhongang Qi, Ying Shan, and Xi Li. Layoutdiffusion: Controllable diffusion model for layout-to-image generation. In *Proceedings of the IEEE/CVF Conference on Computer Vision and Pattern Recognition (CVPR)*, pages 22490–22499, June 2023. [1](#), [3](#), [6](#), [14](#), [17](#)

## A. Implementation and Evaluation Details

### A.1. Design of STAY Diffusion’s Network Blocks

We illustrate the design of the Layout Diffusion Resblock and the Diffusion StyledMaskAttnBlock in Fig. 8. In the Layout Diffusion Resblock (see Fig. 8(a)), we replace the Group Normalization [48] layers with novel Edge-Aware Normalization (EA Norm) layers, and the updated object masks  $M^{j+1}$  are predicted at the end of the block. Before passing to the next block, we follow the design in [41] to further refine  $M_i^{j+1}$  with  $M_i^{j+1} = (1 - \eta) \cdot M_i^0 + \eta \cdot M_i^{j+1}$ , where  $\eta$  is a learnable weight and  $i, j$  are the object and ResBlock indices, respectively. Note that the  $M^j$  used for the current Resblock is the weighted sum of the initial object masks  $M^0$  and the predicted masks  $M^j$  from the previous Resblock. As for the Diffusion StyledMaskAttnBlock, we replace the original self-attention by the proposed Styled-Mask Attention (SM Attention) layer as shown in Fig. 8(b).

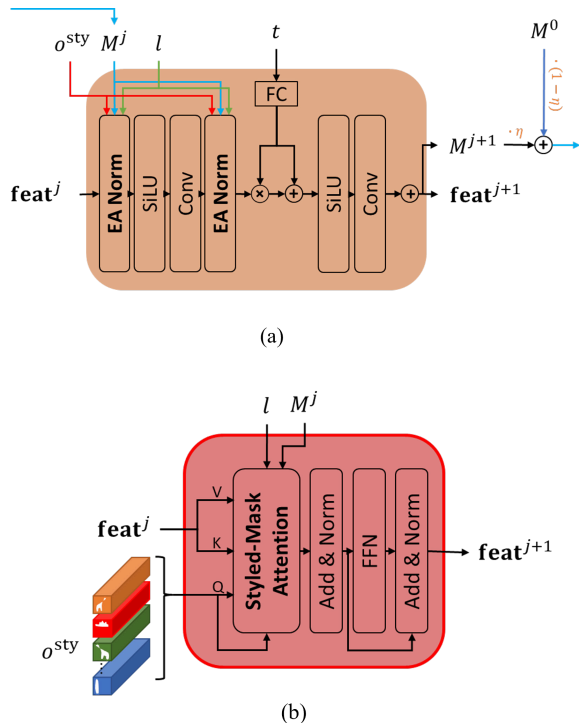


Figure 8. The design of (a) the Layout Diffusion Resblock and (b) the Diffusion StyledMaskAttnBlock, respectively.

### A.2. Evaluation Images of Compared Methods

For layout-to-image (L2I) synthesis methods, we acquired images of LostGAN v2 [41], PLGAN [44], LAMA [21], TwFA [50], LayoutDiffuse [6], and LayoutDiffusion (LayoutDM) [56] by sampling from the checkpoints released by the authors. Since there is no publicly available

Table 4. The reported FID and YoloScore (AP) in Tab. 2 of GLIGEN [20] and our reproduced results (marked with \*).

Methods	FID ↓	Yolo ↑
GLIGEN [20]	21.04	22.4
GLIGEN [20]*	21.30	23.0

COCO-stuff checkpoint for GLIGEN [20], we followed the setting described by the authors to train a model on COCO-stuff based on LDM [34]. We then sampled from this model, following the instructions of the authors such as using scheduled sampling. Our evaluation results on the sampled images (cf. Tab. 1 and Tab. 6) closely matched the reported numbers in GLIGEN (cf. Tab. 2<sup>1</sup> in their main paper). We also provide a quick comparison in Tab. 4. As for Visual Genome (VG), we sampled from the checkpoint provided by the authors of GLIGEN.

For semantic image synthesis benchmark methods, we selected ControlNet-v1.1 [52], FreestyleNet [49], PITI [45] and SDM [46] for evaluation. We used the checkpoints released by the authors and gave the models different sets of semantic maps (i.e., the ground truth map (GT), the self-supervised map with overlapping objects from Tab. 2(a) (Base) and the self-supervised map from our full model (Ours)) to generate images for evaluation.

### A.3. Training and Sampling Details for STAY Diffusion

We reported the used hyperparameters of STAY Diffusion for training and sampling in Tab. 5. For models trained at resolution  $256 \times 256$ , we used four Tesla A100 for training. For models trained at resolution  $128 \times 128$ , we used four Tesla V100 for training. Finally, a Tesla V100 was used to sample images from both resolutions.

## B. Interactivity of STAY Diffusion

We demonstrate the interactivity of STAY Diffusion in Fig. 9. Although imperfect, the self-supervised maps generated by STAY Diffusion can help reduce human effort for image labeling or provide more comprehensive information for downstream tasks such as image blending. As shown in Fig. 9(a), the mask extracted from STAY Diffusion is more accurately aligned with the object shape than the one drawn from a raw bounding box. Furthermore, in Fig. 9(b), we gradually added an object to the layout to demonstrate that STAY Diffusion can be easily adjusted to reconfigurations.

<sup>1</sup>The authors of GLIGEN refer to COCO-stuff as COCO2017D.

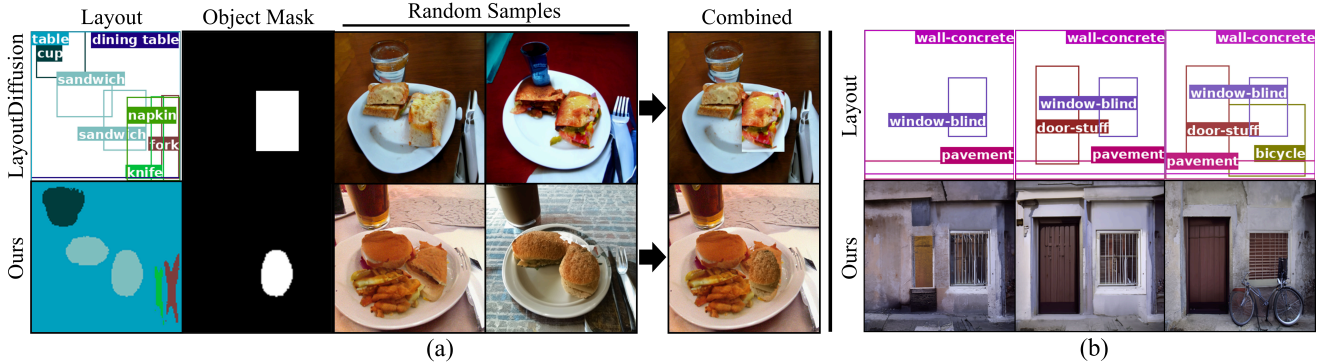


Figure 9. The interactivity of STAY Diffusion. (a) With the self-supervised semantic maps, STAY Diffusion provides more accurate object location for tasks like image blending. (b) STAY Diffusion can adapt to reconfigured layouts.

## C. Additional Results

### C.1. Full Quantitative Results

We reported the full quantitative results on COCO-stuff in Tab. 6 and Visual Genome (VG) in Tab. 7. Note that the YOLOScores are only applicable for COCO-stuff as defined in [21]. As shown in both tables, our STAY Diffusion presents superior performance in image diversity, generation accuracy, and controllability. As for image quality, our method shows comparable results to the previous state-of-the-art (SOTA) in FID and IS.

### C.2. More Visualization Results

We show more visual comparison to previous methods on COCO-stuff in Fig. 10 and Fig. 11, and VG in Fig. 12 and Fig. 13. Additionally, we provided more demonstration of style variations on object appearance in Fig. 14, the learned self-supervised semantic maps and generated images based on the same layout in Fig. 15, and more visual comparisons between our ablated models in Fig. 16.

### C.3. Additional Results for Mask Clarity

We present the full table of the quantitative results on mask clarity in Tab. 8. As for the visual comparison, we present the generated images from different semantic image synthesis and our STAY Diffusion in Fig. 17. It can be clearly seen that the self-supervised maps from our full model (**Ours**) produce images with recognizable objects and higher quality compared to the self-supervised maps from the **Base** (i.e., Tab. 2(a)). This again highlights the importance of the mask clarity. Moreover, it is evident that the semantic image synthesis methods highly rely on precisely labeled maps. When those are not available, their generation quality drops severely. This observation is also aligned with the quantitative results in Tab. 8. On the other hand, our STAY Diffusion still produces images with superior quality in this case due to the proposed EA Norm and SM Attention in Sec. 3.

Table 5. The used hyperparameters for the proposed STAY Diffusion in Sec. 4 experiments.

<b>Dataset Model</b>	<b>COCO-stuff 256×256 STAY Diffusion</b>	<b>COCO-stuff 128×128 STAY Diffusion</b>	<b>VG 256×256 STAY Diffusion</b>
<b>Layout-Conditional Diffusion Model</b>			
In Channels	3	3	3
Hidden Channels	256	128	256
Channel Multiply	1,1,2,2,4,4	1,1,2,3,4	1,1,2,2,4,4
Number of Residual Blocks	2	2	2
Dropout	0	0	0
Diffusion Steps	1000	1000	1000
Noise Schedule	linear	linear	linear
$\lambda$	0.001	0.001	0.001
<b>Object Representation</b>			
Class Embedding Dimension	180	180	180
Style Embedding Dimension	128	128	128
Maximum Number of Objects	8	8	8
Maximum Number of Class Id	184	184	179
<b>Edge-Aware Normalization Module</b>			
$\alpha$	0.5	0.5	0.5
<b>Styled-Mask Attention Module</b>			
Attention Method	Styled-Mask	Styled-Mask	Styled-Mask
Number of Head Channels	64	64	64
<b>Training Hyperparameters</b>			
Total Batch Size	32	32	32
Number of GPUs	4	4	4
Learning Rate	1e-4	1e-4	1e-4
Mixed Precision Training	No	No	No
Weight Decay	0	0	0
EMA Rate	0.9999	0.9999	0.9999
Iterations	1.25M	600K	1.45M
<b>Sampling Hyperparameters</b>			
Total Batch Size	4	8	4
Number of GPUs	1	1	1
Classifier-free Guidance $s$	1.5	1.5	1.0
Use DPM-Solver	True	True	True
DPM-Solver Algorithm	dpmsolver++	dpmsolver++	dpmsolver++
DPM-Solver Type	dpmsolver	dpmsolver	dpmsolver
DPM-Solver Skip Type	time_uniform	time_uniform	time_uniform
DPM-Solver Step Method	singlestep	singlestep	singlestep
DPM-Solver ODE Order	3	3	2
DPM-Solver Timesteps	50	50	50



Table 6. Quantitative results on COCO-stuff at resolution  $256 \times 256$ . The proposed STAY Diffusion outperforms LayoutDiffusion (LayoutDM) in diversity, accuracy and controllability metrics while maintaining close quality performance.

Methods	Coco-Stuff				
	FID ↓	IS ↑	DS ↑	CAS ↑	Yolo ↑
LostGAN v2 [41]	33.17	18.08±0.46	0.55±0.10	33.17	15.0
PLGAN [44]	30.67	18.92±0.65	0.52±0.10	29.15	13.6
LAMA [21]	33.00	19.77±0.66	0.48±0.12	9.97	20.4
TwFA [50]	23.78	23.02±0.94	0.43±0.13	20.09	23.9
LayoutDiffuse [6]	22.41	27.09±0.07	0.58±0.11	31.80	23.7
GLIGEN [20]	21.30	<b>27.71±0.79</b>	0.57±0.09	34.41	23.0
LayoutDM [56]	<b>15.74</b>	26.01±0.84	0.58±0.09	35.69	27.2
<b>Ours</b>	17.43	26.08±0.76	<b>0.59±0.09</b>	<b>37.18</b>	<b>29.5</b>

Table 7. Quantitative results on Visual Genome (VG) at resolution  $256 \times 256$ . The proposed STAY Diffusion outperforms LayoutDiffusion (LayoutDM) in diversity, accuracy and controllability metrics while maintaining close quality performance.

Methods	VG			
	FID ↓	IS ↑	DS ↑	CAS ↑
LostGAN v2 [41]	34.92	14.01±0.81	0.53±0.01	24.40
PLGAN [44]	-	-	-	-
LAMA [21]	38.51	13.70±0.76	0.54±0.10	24.16
TwFA [50]	18.57	17.75±0.68	0.50±0.10	18.30
LayoutDiffuse [6]	22.45	<b>22.89±1.69</b>	0.56±0.10	25.05
GLIGEN [20]	23.42	21.84±1.38	0.60±0.09	25.49
LayoutDM [56]	<b>15.26</b>	21.94±1.28	0.61±0.10	26.84
<b>Ours</b>	18.02	18.56±0.91	<b>0.65±0.08</b>	<b>27.23</b>

Table 8. Quantitative results of mask clarity on COCO-stuff. When GT maps are absent, the images generated from the self-supervised maps of our full model (**Ours**) outperform other baseline methods in quality and controllability metrics, highlighting the importance of clear masks.

Methods	Mask	FID ↓	IS ↑	DS ↑	CAS ↑	Yolo ↑
ControlNet-v1.1 [52]	GT	32.24	24.80±1.44	0.54±0.08	22.43	25.6
FreestyleNet [49]	GT	14.80	30.06±0.92	0.50±0.09	36.67	42.9
PITI [45]	GT	15.22	28.08±1.11	0.45±0.12	37.20	34.8
SDM [46]	GT	20.79	23.82±0.53	0.65±0.18	36.42	26.9
ControlNet-v1.1 [52]	Base	64.29	17.47±0.49	0.59±0.09	9.36	4.1
FreestyleNet [49]	Base	37.21	20.40±0.73	0.50±0.09	21.54	12.9
PITI [45]	Base	61.01	12.90±0.39	0.46±0.12	14.02	4.7
SDM [46]	Base	40.08	15.41±0.26	0.69±0.18	19.29	10.5
ControlNet-v1.1 [52]	Ours	50.25	20.65±0.93	0.60±0.09	15.38	6.5
FreestyleNet [49]	Ours	32.95	22.59±0.66	0.56±0.10	26.52	13.8
PITI [45]	Ours	37.41	17.24±0.91	0.53±0.13	18.63	12.0
SDM [46]	Ours	35.53	17.70±0.72	<b>0.69±0.19</b>	22.69	13.5
<b>Ours</b>	Ours	<b>17.43</b>	<b>26.08±0.76</b>	0.59±0.09	<b>37.18</b>	<b>29.5</b>



Figure 10. More comparison with previous methods on COCO-stuff  $256 \times 256$ . Zoom in for better view.

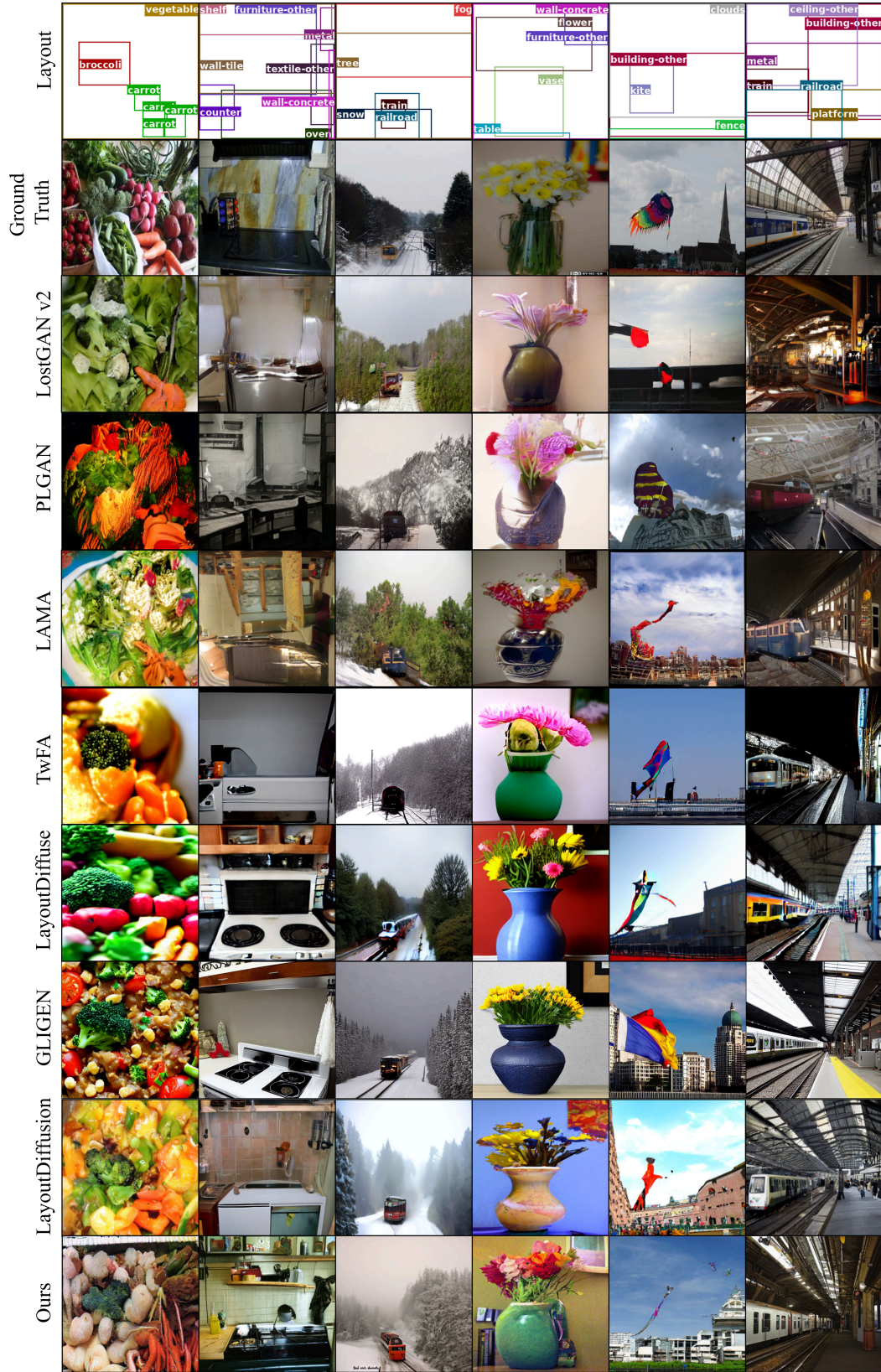


Figure 11. More comparison with previous methods on COCO-stuff  $256 \times 256$ . Zoom in for better view.

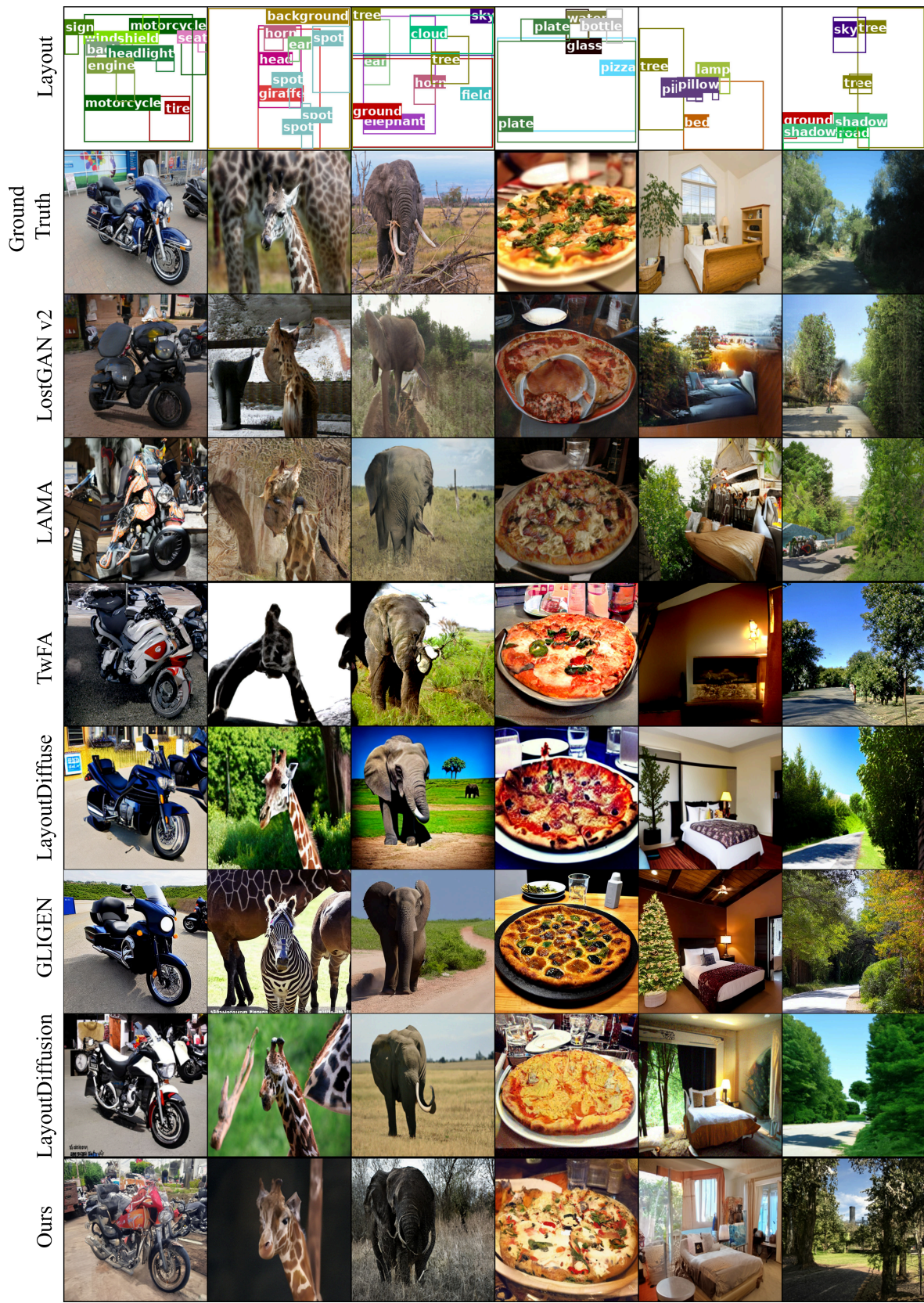


Figure 12. Visual comparison with previous methods on VG  $256 \times 256$ .



Figure 13. Visual comparison with previous methods on VG  $256 \times 256$ .

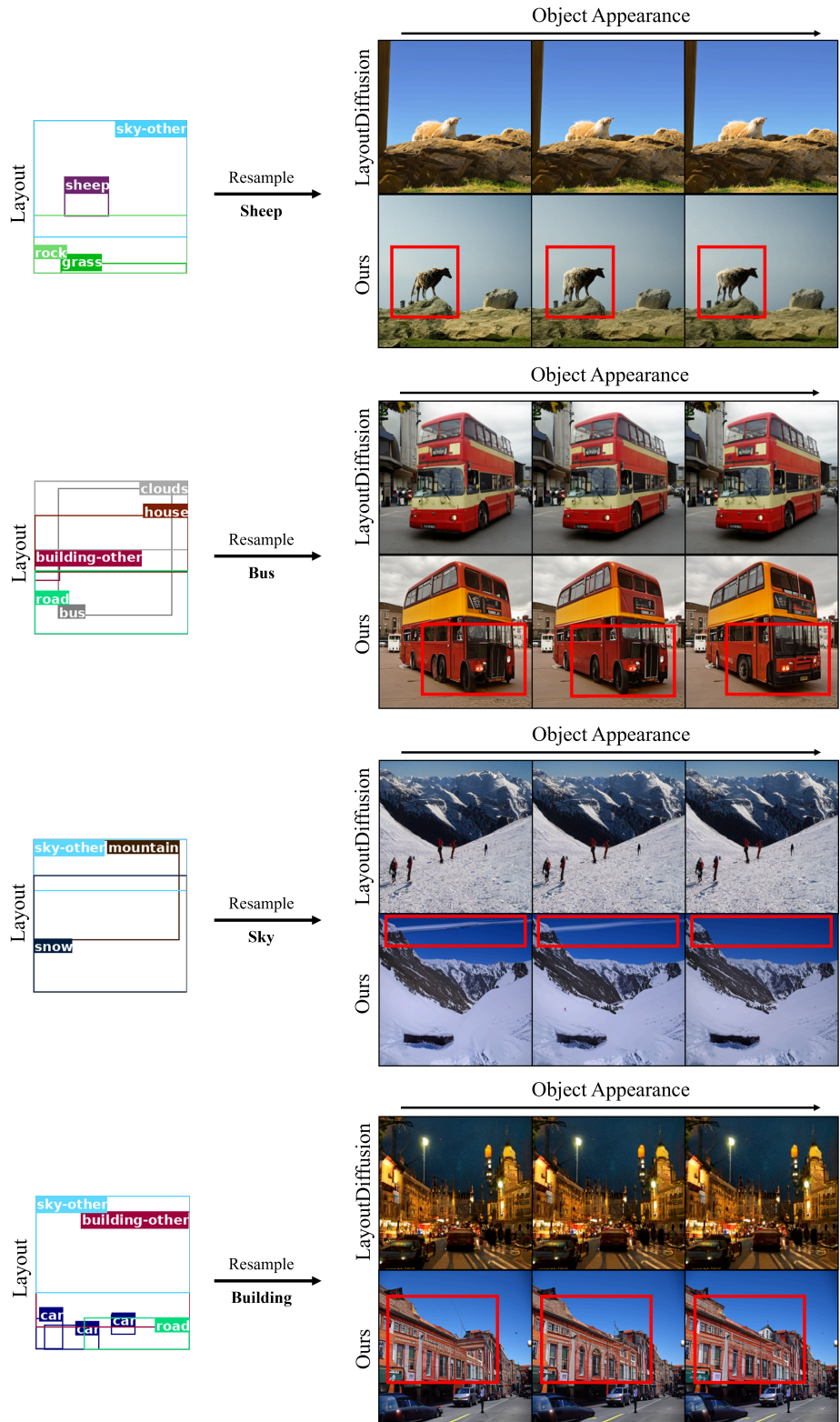


Figure 14. The demonstration of fine-grained style variations offered by our STAY Diffusion. Note that only one object is resampled in each image (Zoom in for better view).

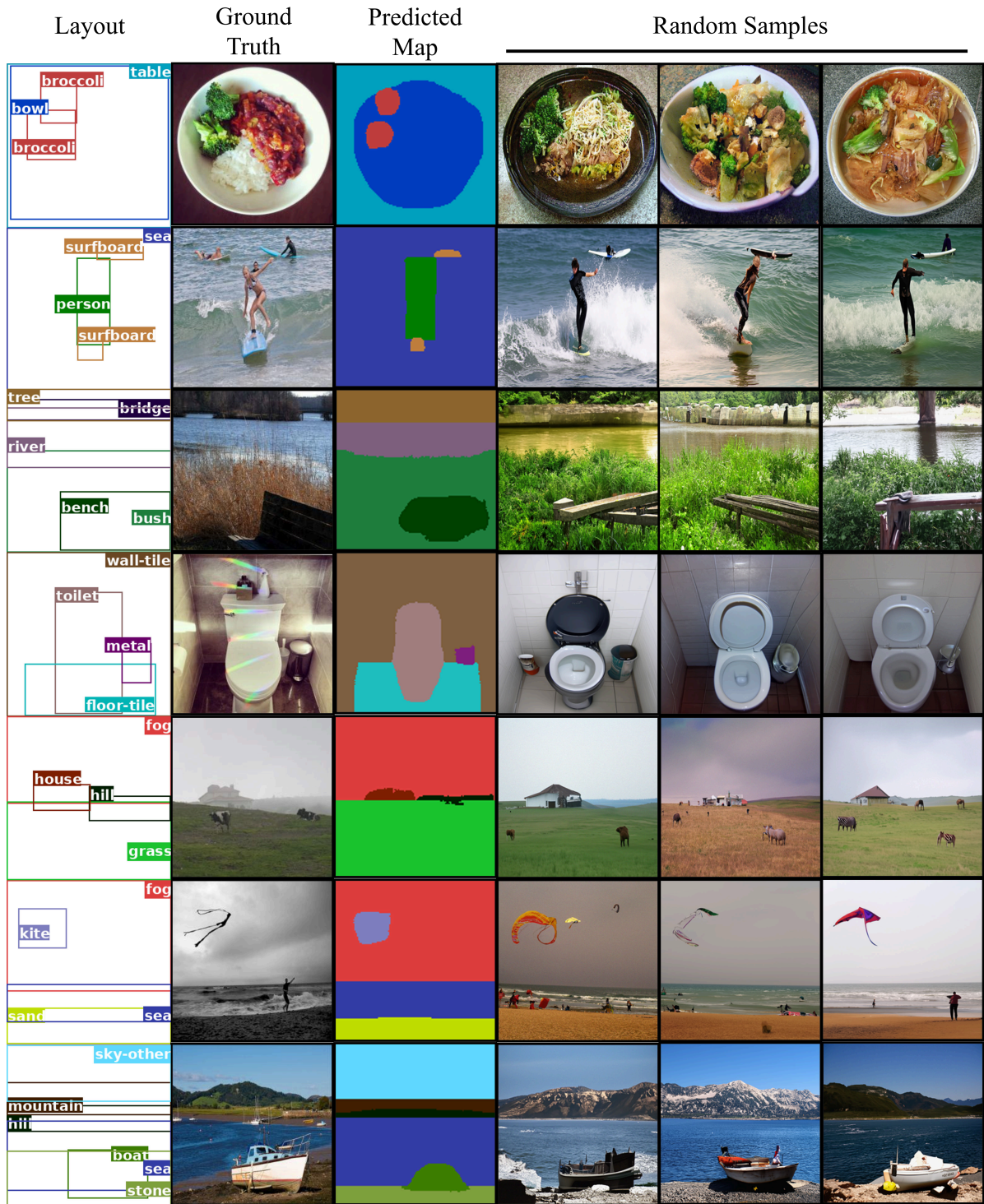


Figure 15. The demonstration of self-supervised semantic maps learned by our STAY Diffusion.

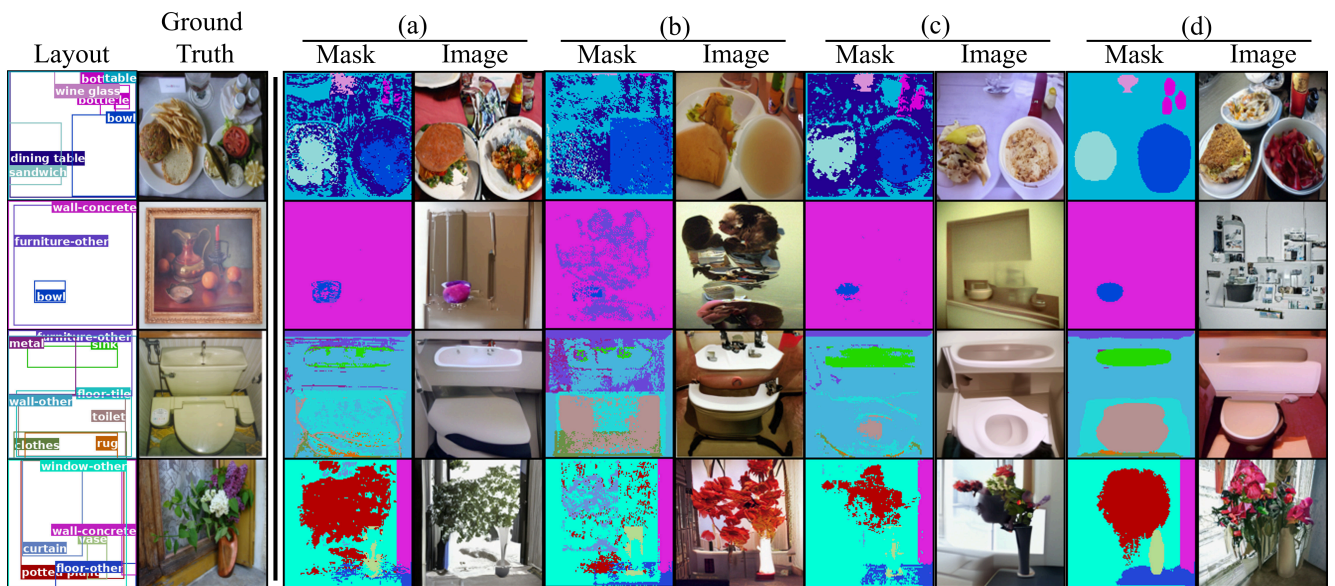


Figure 16. The generated images and their predicted self-supervised semantic maps from ablated models mentioned in Sec. 4.5. (a) ISLA Norm + Self Attention. (b) EA Norm + Self Attention. (c) ISLA Norm + SM Attention. (d) EA Norm + SM Attention.



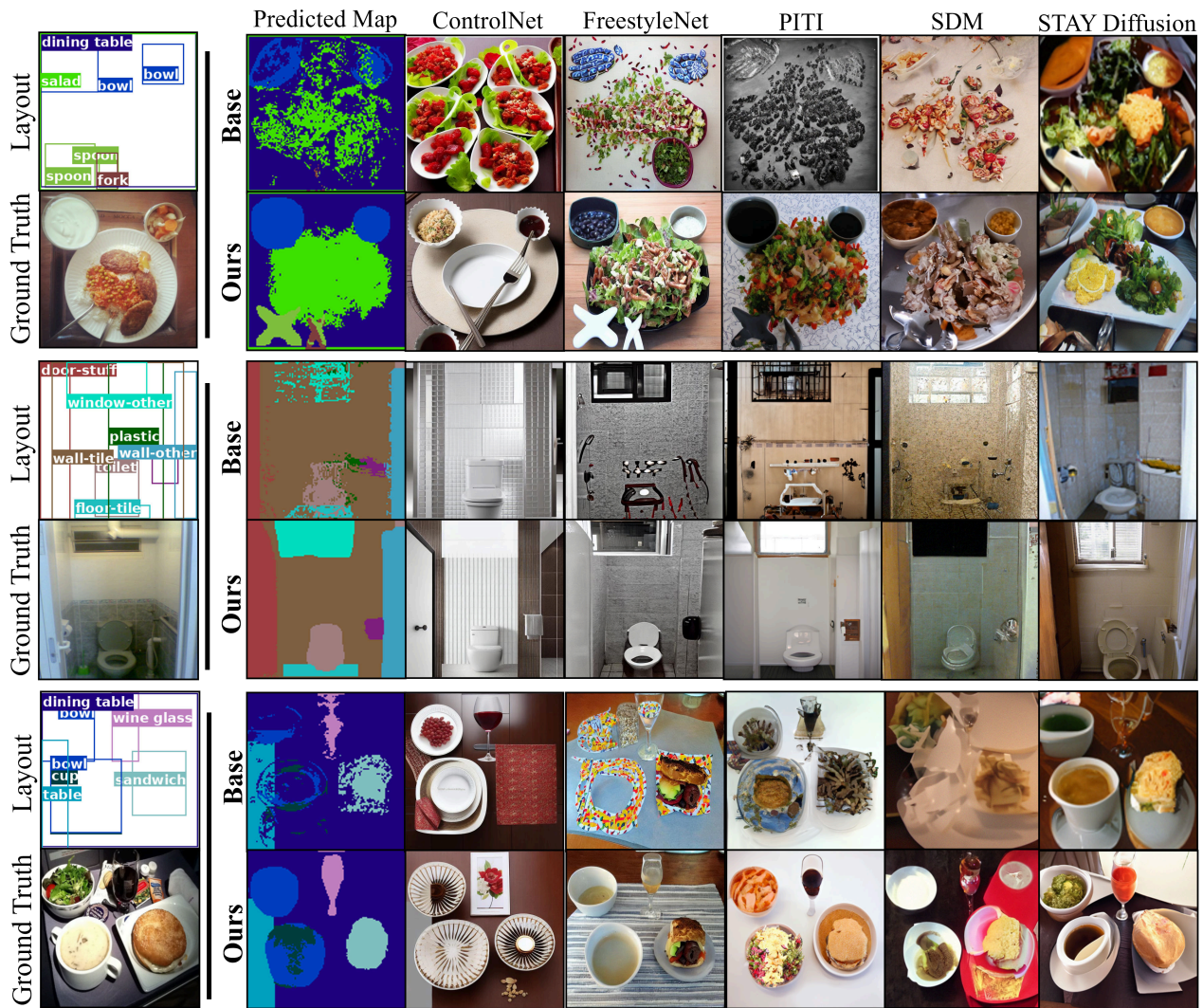


Figure 17. The visual comparison of images generated from different semantic image synthesis methods and our STAY Diffusion. Note that **Base** indicates the baseline self-supervised map from Tab. 2 setting (a) and **Ours** indicates the self-supervised map from the full model (i.e., Tab. 2 setting (d)).